LDHA protects vascular endothelial cells from oxidative stress-induced mitochondrial damage via HIF-1α activation and glycolytic reprogramming

BEIBEI DAI[1-3*], LILI YANG[4*], YU ZHANG[4] and AIYONG YU[4]

[1]Department of Ultrasound, Obstetrics and Gynecology Hospital of Fudan University, Shanghai 200433, P.R. China; [2]Shanghai Key Laboratory of Reproduction and Development, Obstetrics and Gynecology Hospital of Fudan University, Shanghai 200433, P.R. China; [3]Shanghai Key Laboratory of Female Reproductive Endocrine Related Diseases, Obstetrics and Gynecology Hospital of Fudan University, Shanghai 200433, P.R. China; [4]Department of Neurology, Songjiang Hospital Affiliated to Shanghai Jiao Tong University School of Medicine, Shanghai 201699, P.R. China

Received February 19, 2025; Accepted September 5, 2026

DOI: 10.3892/mmr.2026.13851

Abstract. Oxidative stress-induced damage contributes to endothelial dysfunction, a key feature in the pathogenesis of cerebral aneurysms (CAs). Lactate dehydrogenase A (LDHA) serves a crucial role in regulating metabolic adaptation under stress. The present study aimed to explore the protective effects of LDHA overexpression on vascular endothelial cells (VECs) under oxidative stress induced by hydrogen peroxide (H_2O_2). VECs were exposed to 0.5 mM H_2O_2 in an oxygen-glucose deprivation/reperfusion (OGD/R) model to induce oxidative stress, mimicking conditions relevant to CA. LDHA overexpression was achieved using a plasmid vector. Subsequently, western blotting, flow cytometry, reverse transcription-quantitative polymerase chain reaction, transmission electron microscopy and JC-1 staining were used to assess apoptosis, mitochondrial function, glycolysis and oxidative stress markers. Extracellular acidification rate was measured to evaluate glycolytic activity. The results revealed that LDHA overexpression reduced oxidative stress-induced apoptosis and mitochondrial damage in VECs, as evidenced by decreased caspase activation (caspase-3, caspase-9), preserved mitochondrial structure and improved mitochondrial membrane potential. Additionally, LDHA overexpression mitigated reactive oxygen species production and activated hypoxia-inducible factor 1α (HIF-1α). It also increased the expression of glycolytic genes (hexokinase 2, phosphoglucomutase 5 and pyruvate kinase M) and upregulated the lactate transporter monocarboxylate transporter 4, while decreasing succinate levels. Furthermore, LDHA overexpression enhanced NADPH levels and glucose-6-phosphate dehydrogenase activity, indicating the activation of the pentose phosphate pathway to maintain redox balance. In conclusion, LDHA may protect VECs from mitochondrial dysfunction and oxidative damage in the context of CA by enhancing glycolytic metabolism and HIF-1α signaling. LDHA could therefore serve as a possible therapeutic target for the treatment and prevention of CAs.

Correspondence to: Dr Aiyong Yu or Dr Yu Zhang, Department of Neurology, Songjiang Hospital Affiliated to Shanghai Jiao Tong University School of Medicine, 748 Zhongshan Middle Road, Songjiang, Shanghai 201699, P.R. China
E-mail: aiyong07@sohu.com
E-mail: zhangyufendou@163.com

*Contributed equally

Key words: lactate dehydrogenase A, mitochondrial damage, cerebral aneurysms, hypoxia-inducible factor 1α, glycolytic reprogramming

Introduction

Cerebral aneurysms (CAs) are a pathological condition characterized by a bulging or weakened region in the arterial wall of the brain, which increases the risk of rupture (1). The rupture of CAs typically leads to the compression of surrounding brain tissue, potentially impairing basic brain functions (2). Aneurysmal subarachnoid hemorrhage (aSAH) is responsible for ~5% of all strokes and carries a high mortality rate ranging between 22 and 50% (3). With advancements in scientific technologies, the detection rate of CAs has gradually increased. Common diagnostic techniques for CAs involve magnetic resonance imaging and computed tomography scans, and angiography (4). For smaller, asymptomatic aneurysms, a conservative approach focused on observation is often employed (5). Surgical interventions, such as aneurysm clipping and endovascular embolization, are commonly used to seal off larger or symptomatic aneurysms and prevent rupture (6). Notably, control of blood pressure is widely recognized as a key factor in preventing intracranial aneurysm (IA) rupture; therefore, blood pressure management and adjunctive treatments to prevent thrombosis are frequently used as therapeutic strategies (7).

Mitochondrial damage can lead to disturbances in energy metabolism, impairing the normal function of vascular smooth muscle cells and compromising the stability of the vessel wall (8). The formation of CAs is often associated with vascular wall remodeling; this process involves smooth muscle cell migration and proliferation, as well as the upregulation of matrix metalloproteinases (MMPs), all contributing to vascular wall expansion (9). Mitochondrial damage impairs the normal function of these cells, particularly affecting the proliferation, migration and matrix synthesis of vascular smooth muscle cells. Research has suggested that mitochondrial repair represents a potential pharmacological target for cerebral ischemia. It offers new therapeutic directions for related diseases, including transient ischemic attacks, aneurysms and strokes (10). Zhao *et al* (11) demonstrated that microRNA-29a, by targeting Mcl-1, can regulate the mitochondrial apoptotic pathway and promote the progression of CAs, making it a potential therapeutic target for aneurysm treatment. Furthermore, Wang *et al* (12) utilized Mendelian randomization analysis to identify mitochondrial-associated proteins, such as CCDC90B, tRNA PusA and AIF1, as factors linked to an increased risk of CAs. Notably, these factors were particularly associated with aSAH. These outcomes provide novel perspectives into the pathogenesis and potential treatment strategies for CAs.

Lactate dehydrogenase A (*LDHA*) encodes the A subunit of LDH, an enzyme that facilitates anaerobic glycolysis; it catalyzes the reversible conversion of pyruvate to lactate while simultaneously reducing NADH to NAD (13). A previous study showed that LCN2 promotes vascular remodeling in pulmonary hypertension (PH) via the Akt-hypoxia-inducible factor 1α (HIF-1α)-LDHA axis (14). Furthermore, Wu *et al* (15) showed that LDHA-mediated lactate generation promotes pulmonary vasculature remodeling in PH by activating the Akt pathway. This finding highlights the critical function of LDHA in vascular remodeling and metabolic reprogramming in PH. Previous research has also explored the effects of lactate metabolism-related genes, LDHA and vascular endothelial growth factor A (VEGFA), on vascular endothelial cells (VECs) under oxidative stress (16). Oxidative stress promotes a metabolic shift towards glycolysis by regulating LDHA expression, glycolytic activity and lactate production. Upregulation of LDHA can enhance cell survival and reduce apoptosis, whereas knockdown of VEGFA leads to the opposite effects. Notably, oxidative stress contributes to the formation and rupture of CAs by damaging endothelial cells and promoting the transformation of smooth muscle cells into an inflammatory phenotype. It also initiates inflammatory responses and activates MMPs through the generation of free radicals (17). The present study initially exposed VECs to hydrogen peroxide (H_2O_2)-induced oxidative stress and then subjected them to oxygen-glucose deprivation/reperfusion (OGD/R) treatment to mimic ischemia-reperfusion damage. This approach allows for the modeling of the pathological conditions of VECs in CAs. A previous study has shown that LDHA can exacerbate myocardial ischemia-reperfusion injury by inducing the lactylation of NOD-, LRR- and pyrin domain-containing protein 3 (18).

The current study aimed to examine the function of LDHA in the pathophysiology of CAs, particularly focusing on its impacts on mitochondrial function, oxidative stress and metabolic reprogramming in VECs. Given the critical role of oxidative stress and mitochondrial damage in aneurysm progression, it was hypothesized that LDHA overexpression may mitigate these adverse effects. This protective effect could potentially be achieved by enhancing antioxidant defense, preserving mitochondrial integrity and promoting glycolytic activity. Additionally, the potential participation of the HIF-1α pathway in mediating the protective effects of LDHA under oxidative conditions was explored. The findings of the present study may provide novel insights into the molecular mechanisms underlying aneurysm development. They could also identify potential therapeutic targets for CAs and related disorders, such as subarachnoid hemorrhage.

Materials and methods

Cell line and culture. The human umbilical VEC-derived cell line EA.hy926 (cat. no. SCSP-5285) was provided by The Cell Bank of Type Culture Collection of The Chinese Academy of Sciences. The VECs were cultivated in Dulbecco's Modified Eagle Medium (DMEM; Gibco; Thermo Fisher Scientific, Inc.) supplemented with 1% penicillin-streptomycin (Gibco; Thermo Fisher Scientific, Inc.) and 10% fetal bovine serum (Gibco; Thermo Fisher Scientific, Inc.) in a humidified atmosphere containing 5% CO_2 at 37˚C. The cells were passaged when they reached 80-90% confluence and the medium was changed every 2 days. All experiments were conducted using cells between passages 3 and 5 after thawing. To investigate the roles of HIF-1α signaling and glycolysis, the cells were treated with 20 μM PX478 (MedChemExpress), a HIF-1α inhibitor, for 20 h at 37˚C, or 2 mM 2-deoxy-D-glucose (2-DG; MedChemExpress), a glycolysis inhibitor, for 24 h at 37˚C, under oxidative stress conditions induced by preconditioning with 0.5 mM H_2O_2 for 12 h at 37˚C, followed by OGD/R (6-h OGD at 37˚C and 24-h reoxygenation at 37˚C) [hereafter referred to as 0.5 mM H_2O_2 (OGD/R)].

Oxidative stress and ischemia-reperfusion injury model generation in VECs. The pathogenesis of CAs is multifactorial, with oxidative stress being a key factor. Oxidative stress can lead to endothelial dysfunction, inflammation and vascular wall remodeling, all of which contribute to the formation and rupture of aneurysms (19). Oxidative stress is often induced by hemodynamic changes, such as turbulent blood flow and wall shear stress (WSS), which are common in aneurysmal regions (20). Additionally, ischemia-reperfusion injury, a condition where blood flow is temporarily interrupted and then restored, is a notable contributor to oxidative stress and mitochondrial dysfunction in CAs. The OGD/R model is widely used to simulate ischemia-reperfusion injury *in vitro*; this model mimics the conditions of transient cerebral ischemia followed by reperfusion, which is relevant to the pathophysiology of CAs (21,22). The present study employed a combined treatment of 0.5 mM H_2O_2 and OGD/R to induce oxidative stress in VECs, thereby mimicking ischemia-reperfusion injury. VECs, as critical cellular components of the cerebral arterial wall, serve a pivotal role in maintaining vascular

integrity and their dysfunction is closely associated with aneurysm pathogenesis. VECs were subjected to oxidative stress via treatment with 0.5 mM H_2O_2 (OGD/R) to mimic ischemic conditions, as previously described by Wu *et al* (16). OGD/R involved incubating cells in glucose-free DMEM under hypoxic conditions (1% O_2) for 24 h, followed by reoxygenation with complete DMEM under normoxic conditions (21% O_2) for 24 h.

Cell transfection. VECs were plated in 24-well plates at a density of $2x10^5$ cells/well to achieve optimal confluence for transfection. To regulate LDHA expression, VECs were transfected with an LDHA overexpression plasmid (pcDNA-3.1-LDHA) or with an empty pcDNA-3.1 vector (negative control) (both from Shanghai GenePharma Co., Ltd.). The cells were transfected with 500 ng plasmid in 24-well plates using Lipofectamine® 3000 reagent (Invitrogen; Thermo Fisher Scientific, Inc.) at 37˚C and 5% CO_2 for 6 h according to the manufacturer's instructions. VECs were harvested 48 h post-transfection for further analysis.

Experimental groups. For subsequent experiments, VECs were divided into six groups: i) Control (untreated VECs); ii) 0.5 mM H_2O_2 (OGD/R); iii) 0.5 mM H_2O_2 (OGD/R) + vector (empty pcDNA-3.1 vector); iv) 0.5 mM H_2O_2 (OGD/R) + over-LDHA (pcDNA-3.1-LDHA plasmid); v) 0.5 mM H_2O_2 (OGD/R) + over-LDHA + PX478 (20 μM PX478 treatment); vi) 0.5 mM H_2O_2 (OGD/R) + over-LDHA + 2-DG (2 mM 2-DG treatment).

Reverse transcription-quantitative polymerase chain reaction (RT-qPCR) assay. Total RNA was extracted from VECs using TRIzol® reagent (Invitrogen; Thermo Fisher Scientific, Inc.) according to the manufacturer's guidelines. cDNA synthesis was performed using the PrimeScript RT Reagent Kit (Takara Bio, Inc.) at 37˚C for 15 min, followed by 85˚C for 5 sec, according to the manufacturer's instructions. On a StepOnePlus Real-Time PCR System (Applied Biosystems; Thermo Fisher Scientific, Inc.), qPCR was performed to measure gene expression levels using the SYBR Green PCR Master Mix (Takara Bio, Inc.). The thermocycling conditions were as follows: Initial denaturation at 95˚C for 30 sec, followed by 40 cycles at 95˚C for 5 sec and 60˚C for 30 sec. Gene expression was normalized to the internal control gene β-actin. The $2^{-\Delta\Delta Cq}$ technique was implemented to determine relative expression levels (23). The primer sequences used for amplification are listed in Table I.

Table I. Primer sequences for reverse transcription-quantitative polymerase chain reaction.

Target	Sequence, 5'-3'
LDHA	Forward: TGTCTCTGGCAAAGTGGATATCTT
	Reverse: GACCCACCCATGACAGCTTA
Caspase-3	Forward: TCCTAGCGGATGGGTGCTAT
	Reverse: TCCAGGGATATTCCAGAGTCCA
Caspase-8	Forward: TCACCTTGTGTCTGAGCTGG
	Reverse: TGACCAACTCAAGGGCTCAG
Caspase-9	Forward: AGGCCCCATATGATCGAGGA
	Reverse: TCGACAACTTTGCTGCTTGC
HK2	Forward: TTGTTGCATGAAACTCCGGC
	Reverse: GCTAACTTCGGCCACAGGAT
PGM5	Forward: CTAGCAGGCCCTGGAATCAG
	Reverse: TTCTCCCACCCACCTTCTCC
PKM	Forward: GTGATGTGGCCAATGCAGTC
	Reverse: CTTGAGGCTCGCACAAGTTC
OGDH	Forward: ATCGTGTCACCGACAGGAAC
	Reverse: CGGAACTCCATGCTGGAACA
DLD	Forward: ACAGCGGAAAAATGCAGAGC
	Reverse: ATCCTCCAGGACCAGAACCT
SUCLG2	Forward: ATGGGATCACCAAAGCCTGC
	Reverse: GGGCGACGTTCTCTTGGATA
β-actin	Forward: AGCTCACCATGGATGATGATATCGC
	Reverse: CACATAGGAATCCTTCTGACCCAT

HK2, hexokinase 2; PGM5. phosphoglucomutase 5; PKM, pyruvate kinase M; OGDH, oxoglutarate dehydrogenase; DLD, dihydrolipoamide dehydrogenase; SUCLG2, succinyl-CoA synthetase β subunit.

Western blotting (WB). Protein lysates from VECs were prepared using RIPA lysis buffer (Thermo Fisher Scientific, Inc.) with phosphatase and protease inhibitors, and the BCA Protein Assay Kit (Thermo Fisher Scientific, Inc.) was utilized to calculate the protein concentration. Equal amounts of protein (20-40 μg) were denatured at 95˚C for 5 min in SDS sample buffer and were separated by SDS-polyacrylamide gel electrophoresis on 10-12% polyacrylamide gels, depending on the molecular weight of the target proteins. The proteins were then transferred onto polyvinylidene fluoride membranes (MilliporeSigma) using a wet transfer system at 4˚C. Following transfer, the membranes were blocked with 5% non-fat milk in TBST buffer (20 mM Tris-HCl, 150 mM NaCl, 0.1% Tween-20, pH 7.6) for 1 h at room temperature to reduce nonspecific binding. Subsequently, the membranes were incubated overnight at 4˚C with primary antibodies against the following proteins: LDHA (1:1,000; cat. no. 2012; Cell Signaling Technology, Inc.), caspase-3 (1:5,000; cat. no. ab32351; Abcam), caspase-9 (1:2,000; cat. no. ab202068; Abcam), caspase-8 (1:1,000; cat. no. ab32397; Abcam), cytochrome *c* (Cyt-c; 1:5,000; cat. no. ab133504; Abcam), Mcl-1 (1:1,000; cat. no. ab32087; Abcam), HIF-1α (1:1,000; cat. no. ab51608; Abcam), sodium-calcium exchanger 1 (NCX1; 1:1,000; cat. no. ab177952; Abcam), sodium-proton exchanger 1 (NHE1; 1:1,000; cat. no. ab67313; Abcam) and monocarboxylate transporter 4 (MCT4; 1:1,000; cat. no. ab308528; Abcam), with β-actin (1:1,000; cat. no. ab8227; Abcam) used as an internal loading control for whole-cell and cytoplasmic proteins, and Lamin B1 (1:20,000; cat. no. 12987-1-AP; Wuhan Sanying Biotechnology) used as a nuclear loading control. After primary antibody incubation, the membranes were washed three times with TBST (10 min each) and were then incubated with horseradish peroxidase-conjugated goat anti-rabbit IgG (H+L) secondary antibody (1:10,000; cat. no. ab6721; Abcam) for 1 h at room temperature. After washing again three times in TBST, the protein bands were visualized using enhanced

chemiluminescence detection reagent (Beyotime Institute of Biotechnology), and images were captured using a chemiluminescence imaging system (Bio-Rad Laboratories, Inc.). Band intensities were semi-quantified using ImageJ software (version 1.5.2; National Institutes of Health).

The nuclear and cytoplasmic proteins were extracted using NE-PER Nuclear and Cytoplasmic Extraction Reagents (Thermo Fisher Scientific, Inc.) following the manufacturer's instructions.

Flow cytometry. For flow cytometry, VECs were detached utilizing a trypsin-EDTA solution (Gibco; Thermo Fisher Scientific, Inc.), followed by a wash with phosphate-buffered saline (PBS). The cells ($1x10^6$) were subsequently stained with an Annexin V-fluorescein isothiocyanate/propidium iodide apoptosis detection kit (Beyotime Institute of Biotechnology), in accordance with the manufacturer's instructions. A FACSCalibur flow cytometer (BD Biosciences) was applied for flow cytometric analysis, and FlowJo software (version 10.8.0; BD Biosciences) was used to process and interpret the data.

Observation of mitochondrial morphology. After being cleaned with PBS, VECs were fixed for 48 h at 4˚C with 2.5% glutaraldehyde in phosphate buffer (pH 7.0). After three washes with PBS, the cells were post-fixed with 1% osmium tetroxide in phosphate buffer for 1 h at room temperature. The samples were then washed three times with PBS. After dehydrating the samples with ethanol solution (30-100%), they were transferred to anhydrous acetone for 20 min at room temperature. Subsequently, absolute acetone and the Spurr resin mixture were mixed 1:1(v/v) and allowed to permeate VECs for 1 h at room temperature. The infiltration process continued with a 3-h incubation in a 1:3 mixture of acetone and resin, followed by embedding in pure Spurr resin overnight at room temperature. The embedded samples were placed in capsules containing the embedding medium and polymerized for ~9 h at 70˚C. Ultrathin sections (60-90 nm) were cut from the resin-embedded blocks using a Leica Ultracut microtome (EM UC7; Leica Biosystems). To improve contrast, the sections were first stained for 15 min with 1% uranyl acetate and then for another 15 min with alkaline lead citrate. The stained sections were examined under a transmission electron microscope (HT7700; Hitachi, Ltd.) at x2,500 magnification. Mitochondrial morphology was evaluated for structural damage, such as changes in size, swelling and shape.

Immunofluorescence (IF) staining. VECs were seeded onto glass coverslips in 24-well plates at $5x10^4$ cells/well and allowed to adhere overnight. Following treatment, the cells were fixed with 4% paraformaldehyde for 15 min at room temperature and permeabilized with 0.1% Triton X-100 in PBS for 10 min at room temperature. Non-specific binding was blocked by incubating the cells in 5% bovine serum albumin (BSA; Beyotime Institute of Biotechnology) in PBS for 1 h at room temperature. Subsequently, the cells were treated overnight at 4˚C with anti-HIF-1α primary antibodies (1:500; cat. no. ab51608; Abcam) diluted in 1% BSA blocking buffer. After washing with PBS, the cells were incubated at room temperature for 1 h with Alexa Fluor® 488-conjugated anti-rabbit IgG (1:200; cat. no. ab150077; Abcam). DAPI (1 μg/ml) was employed to counterstain the nuclei for 5 min. Coverslips were mounted on slides with a sealing agent, and images were captured utilizing a DMi8 fluorescence microscope (Leica Biosystems). Fluorescence intensity and colocalization were analyzed using ImageJ software (version 1.5.2; National Institutes of Health). Representative images are displayed and the experiment was conducted in triplicate.

Measurement of reactive oxygen species (ROS), malondialdehyde (MDA) and glutathione (GSH) levels. The ROS, MDA and GSH assay kits (cat nos. E004-1-1, A003-1-2 and A006-2-1, respectively) were purchased from Nanjing Jiancheng Bioengineering Institute, and were conducted in compliance with the manufacturer's guidelines. VECs were plated at a density of $5x10^5$ cells/well in 6-well plates and were cultured overnight for adherence. For ROS detection, the cells were incubated with 10 μM DCFH-DA fluorescent probe, provided in the ROS assay kit, in the dark for 30 min at 37˚C. Subsequently, the cells were washed twice with PBS, and fluorescence intensity was detected using a microplate reader. Furthermore, MDA levels were quantified to assess lipid peroxidation. After treatment, cell lysates were prepared by adding RIPA buffer supplemented with protease inhibitors, and were centrifuged at 12,000 x g for 15 min at 4˚C. The supernatants were processed according to the kit's instructions, and absorbance was measured at 532 nm using a spectrophotometer. VECs were lysed and centrifuged under the same conditions to evaluate GSH levels. Following the kit's instructions, the supernatants were incubated with the supplied reaction mixture, and absorbance was measured at 405 nm to determine GSH concentrations. Using a BCA protein assay kit, the total protein content in the lysates was employed to standardize all of the outcomes.

Determination of pyruvate, lactate, and succinate levels. To assess the levels of pyruvate, lactate and succinate in VECs under oxidative stress, the cells were seeded in 6-well plates ($2x10^5$ cells/well; n=3 wells per experiment) and were first exposed to 0.5 mM H_2O_2 (OGD/R) treatment, then transfected to induce LDHA overexpression. The culture supernatants were collected 48 h after transfection, clarified by centrifugation at 1,500 x g for 10 min at 4˚C, and stored at -80˚C until analysis, and their pyruvate, lactate and succinate concentrations were analyzed utilizing corresponding commercial assay kits according to the manufacturer's recommendations. Pyruvate and lactate assay kits were purchased from Beijing Solarbio Science & Technology Co., Ltd. (cat nos. BC2205 and BC2235, respectively), while the succinate assay kit (cat no. MAK184) was obtained from MilliporeSigma. The levels of pyruvate were measured at 340 nm, lactate at 340 nm and succinate at 570 nm, using a spectrophotometer (BioTeke Corporation). All measurements were conducted in triplicate and the findings were normalized to protein concentration, which was detected by the BCA assay.

Assessment of mitochondrial membrane potential (MMP). MMP in cells subjected to OGD/R treatment was evaluated utilizing the cationic dye JC-1 (cat. no. T3168; Invitrogen; Thermo Fisher Scientific, Inc.), following the manufacturer's guidelines. Briefly, after OGD/R treatment, the cells were

washed twice with PBS to remove any residual medium. Next, VECs were cultured with JC-1 at a final concentration of 10 μg/ml in serum-free medium for 30 min at 37˚C, ensuring proper penetration of the dye into the cells. JC-1 accumulates in the mitochondria in a potential-dependent manner, exhibiting red fluorescence when aggregated in the mitochondria of cells with high membrane potential, and green fluorescence when dissociated in cells with low membrane potential. Following incubation, the JC-1 working solution was removed, and the cells were washed twice with PBS to eliminate any unbound dye. To reduce any background fluorescence and to ensure clear imaging, washing steps were performed gently. Fluorescence images were then captured using a fluorescence microscope (Leica Biosystems) equipped with appropriate filters to detect both red and green fluorescence emissions. Specifically, red fluorescence was observed at 540 nm for excitation and 590 nm for emission, whereas green fluorescence was measured at 485 nm for excitation and 535 nm for emission. Images were captured at x40 magnification, and five randomly selected fields per sample were analyzed to ensure representative results.

Measurement of extracellular acidification rate (ECAR). ECAR was analyzed utilizing a Seahorse XF Analyzer (Agilent Technologies, Inc.) to evaluate metabolic shifts in VECs following H_2O_2 and OGD/R treatment. VECs were sequentially exposed to glucose (10 mM), oligomycin A (Oligo, 1 μM) and 2-DG (50 mM) from the Seahorse XF Glycolysis Stress Test Kit (cat. no. 103020-100; Agilent Technologies, Inc.) at 37˚C; after each injection, ECAR was recorded for three cycles (mix 3 min, measure 3 min each) to assess glycolytic function. Real-time data were collected and plotted as ECAR over time to visualize the cellular metabolic response to the treatments.

Intracellular Ca^{2+} measurement in VECs. To measure intracellular Ca^{2+} levels in VECs under oxidative stress with LDHA overexpression, the cells were seeded in 6-well plates at 70% confluence. Cells were first subjected to 0.5 mM H_2O_2 (OGD/R), then immediately transfected with either an empty vector or an LDHA overexpression plasmid using Lipofectamine 3000 and incubated for 48 h post-transfection. Cells were collected and resuspended in 500 μl calcium assay buffer. The cell suspension was then scraped on ice and centrifuged at 13,000 x g for 10 min at 4˚C to obtain the supernatant. Intracellular Ca^{2+} concentration was determined using the Calcium Detection Assay Kit (cat. no. ab102505; Abcam) according to the manufacturer's instructions, and absorbance was read at 575 nm on a microplate reader. The resulting data were used to assess any alterations in Ca^{2+} homeostasis due to LDHA overexpression under oxidative stress conditions.

Measurement of NAD^+ and NADH levels. NAD^+ and NADH concentrations were assessed using the NAD^+/NADH Quantification Colorimetric Assay Kit (cat no. ab65348; Abcam) according to the manufacturer's protocol. After plating VECs at a density of $5x10^5$ cells/well in 6-well plates, they were lysed utilizing RIPA buffer (Beyotime Institute of Biotechnology), containing phosphatase and protease inhibitors, and rinsed with PBS. The lysates were then homogenized in 100 μl NAD^+ or NADH extraction buffer. The absorbance of the supernatant was detected at 450 nm utilizing a microplate reader, and the NAD^+ and NADH levels were calculated from the standard curve.

Measurement of NADPH content. NADPH levels in VECs following OGD/R treatment were measured using the NADPH Assay Kit (cat no. S0179; Beyotime Institute of Biotechnology) according to the manufacturer's protocol. VECs were seeded in 6-well plates at $5x10^5$ cells/well and allowed to adhere overnight. Following treatment with the extraction buffer, cells were centrifuged at 10,000 x g for 10 min at 4˚C. The resulting supernatant was incubated for 30 min at 60˚C to degrade $NADP^+$. The supernatant was then cooled on ice, combined with a working solution and incubated for 20 min at 37˚C. The absorbance was measured at 450 nm using a microplate reader.

Determination of glucose-6-phosphate dehydrogenase (G6PDH) activity. The activity of G6PDH in cells was measured using a commercial G6PDH Assay Kit (cat no. S0189; Beyotime Institute of Biotechnology) as per the manufacturer's instructions. For 10 min, cells ($5x10^5$ cells/well; 6-well plates) were centrifuged at 12,000 x g at 4˚C after being treated with the extraction solution. The supernatant (50 μl) was then transferred to a 96-well plate, followed by the addition of 50 μl G6PDH working solution, and was incubated in the dark for 10 min at room temperature. The absorbance was determined at 450 nm using a microplate reader.

Statistical analysis. R language (version 4.3.1; R Foundation for Statistical Computing; https://www.r-project.org/) was used to examine the data. The data are presented as the mean ± SD and all experiments were performed in triplicate. The Student's t-test was used to assess differences between two groups, while one-way ANOVA with Tukey's post hoc test determined differences among multiple groups. $P<0.05$ was considered to indicate significant differences.

Results

Oxidative stress induces apoptosis and mitochondrial pathway activation in VECs. Flow cytometric analysis revealed a significant increase in apoptosis in VECs following treatment with 0.5 mM H_2O_2 (OGD/R) compared with that in the control group (Fig. 1A). To explore the molecular mechanisms, the expression levels of apoptosis-associated factors, including caspase-3, caspase-8 and caspase-9, were assessed using RT-qPCR and WB. The results demonstrated a marked upregulation of these factors following treatment with 0.5 mM H_2O_2 (OGD/R) compared with those in the control group (Fig. 1B-D). Subsequent WB of mitochondrial pathway-related proteins showed that treatment with 0.5 mM H_2O_2 (OGD/R) conditions increased Cyt-c expression while suppressing Mcl-1 expression (Fig. 1E and F). These findings collectively indicated that oxidative stress may promote apoptosis in VECs, accompanied by the activation of mitochondrial apoptosis-related pathways.

LDHA overexpression mitigates oxidative stress-induced apoptosis and mitochondrial damage in VECs. To investigate the connection between *LDHA* expression, apoptosis and

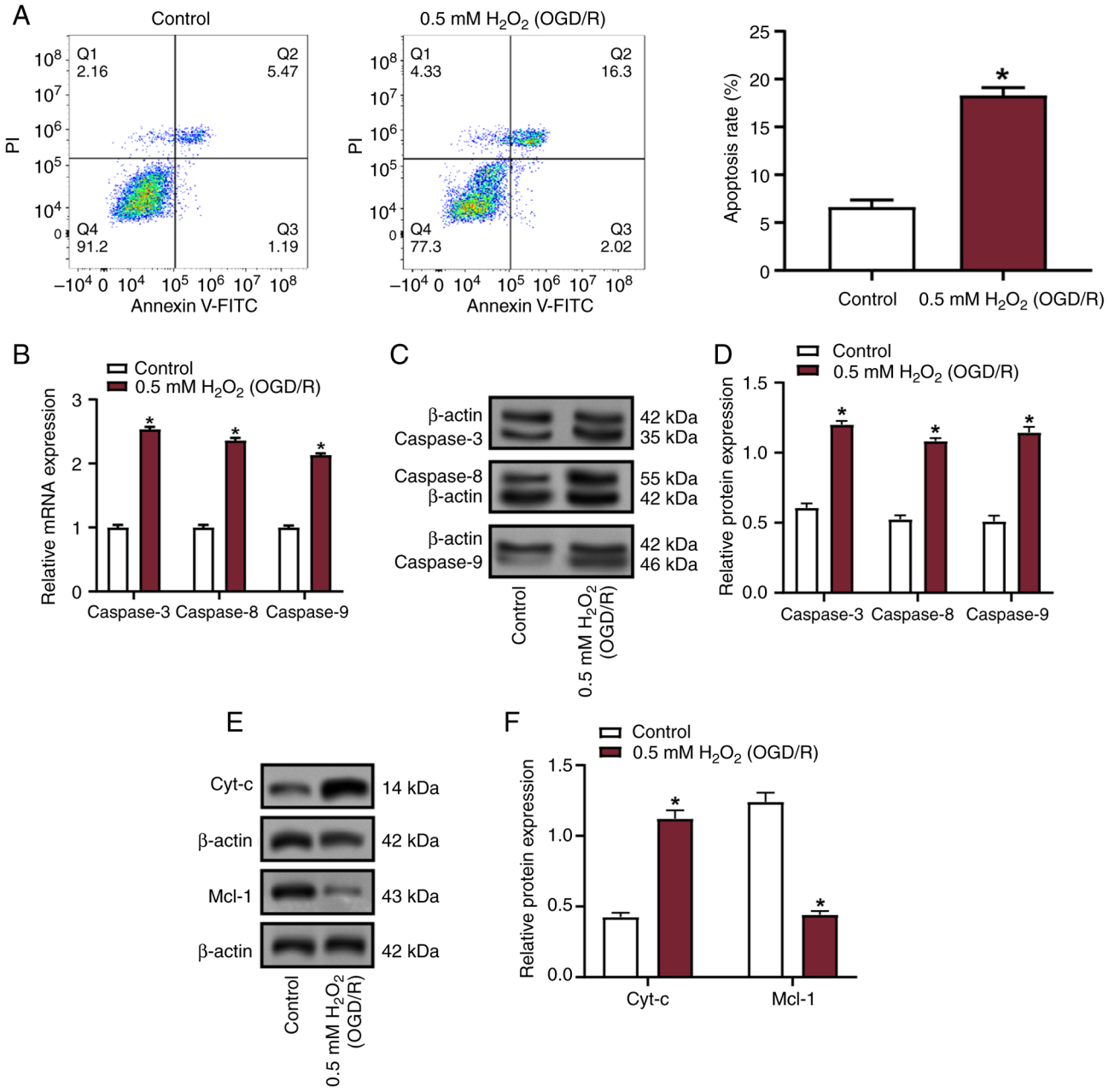

Figure 1. Analysis of apoptosis and expression of apoptosis-related proteins in VECs under oxidative stress conditions. (A) Apoptosis rate of VECs treated with 0.5 mM H_2O_2 under OGD/R conditions, assessed using flow cytometry. (B) Relative mRNA expression levels of caspase-3, caspase-8 and caspase-9 in VECs treated with 0.5 mM H_2O_2 (OGD/R) compared with the control group, measured by reverse transcription-quantitative polymerase chain reaction. mRNA expression levels were normalized to β-actin. (C) WB of caspase-3, caspase-8 and caspase-9 protein expression in VECs treated with 0.5 mM H_2O_2 (OGD/R). The images show representative protein bands with β-actin as the loading control. (D) Semi-quantification of WB data. Protein expression levels are normalized to β-actin. (E) WB of mitochondrial pathway-related proteins Cyt-c and Mcl-1 in VECs treated with 0.5 mM H_2O_2 (OGD/R). (F) Protein expression was normalized to β-actin, and the results are shown as relative expression levels compared with the control group. Data are presented as the mean ± SD of three independent experiments. *P<0.05 vs. control. H_2O_2, hydrogen peroxide; OGD/R, oxygen-glucose deprivation/reperfusion; VECs, vascular endothelial cells; WB, western blotting; PI, propidium iodide; FITC, fluorescein isothiocyanate; Cyt-c, cytochrome *c*.

mitochondrial damage, VECs subjected to 0.5 mM H_2O_2 (OGD/R) conditions were transfected with an LDHA overexpression plasmid. The transfection efficiency was verified by RT-qPCR and WB, which revealed a significant increase in LDHA expression following transfection (Fig. 2A-C). The effects of LDHA overexpression on mitochondrial morphology were further examined using transmission electron microscopy at x2,500 magnification. In the 0.5 mM H_2O_2 (OGD/R) group, mitochondria displayed notable structural damage, including varying sizes, marked swelling, a rounded shape, vacuolar degeneration, and severely reduced, fragmented or absent cristae (Fig. 2D). By contrast, LDHA overexpression improved mitochondrial morphology, with less swelling and better-preserved cristae. WB revealed that 0.5 mM H_2O_2 (OGD/R) treatment increased the expression levels of the pro-apoptotic proteins caspase-3 and Cyt-c, while reducing the expression levels of the anti-apoptotic protein Mcl-1 (Fig. 2E and F). Notably, *LDHA* overexpression reversed these effects, reducing caspase-3 and Cyt-c levels, while reversing Mcl-1 expression. Flow cytometric analysis

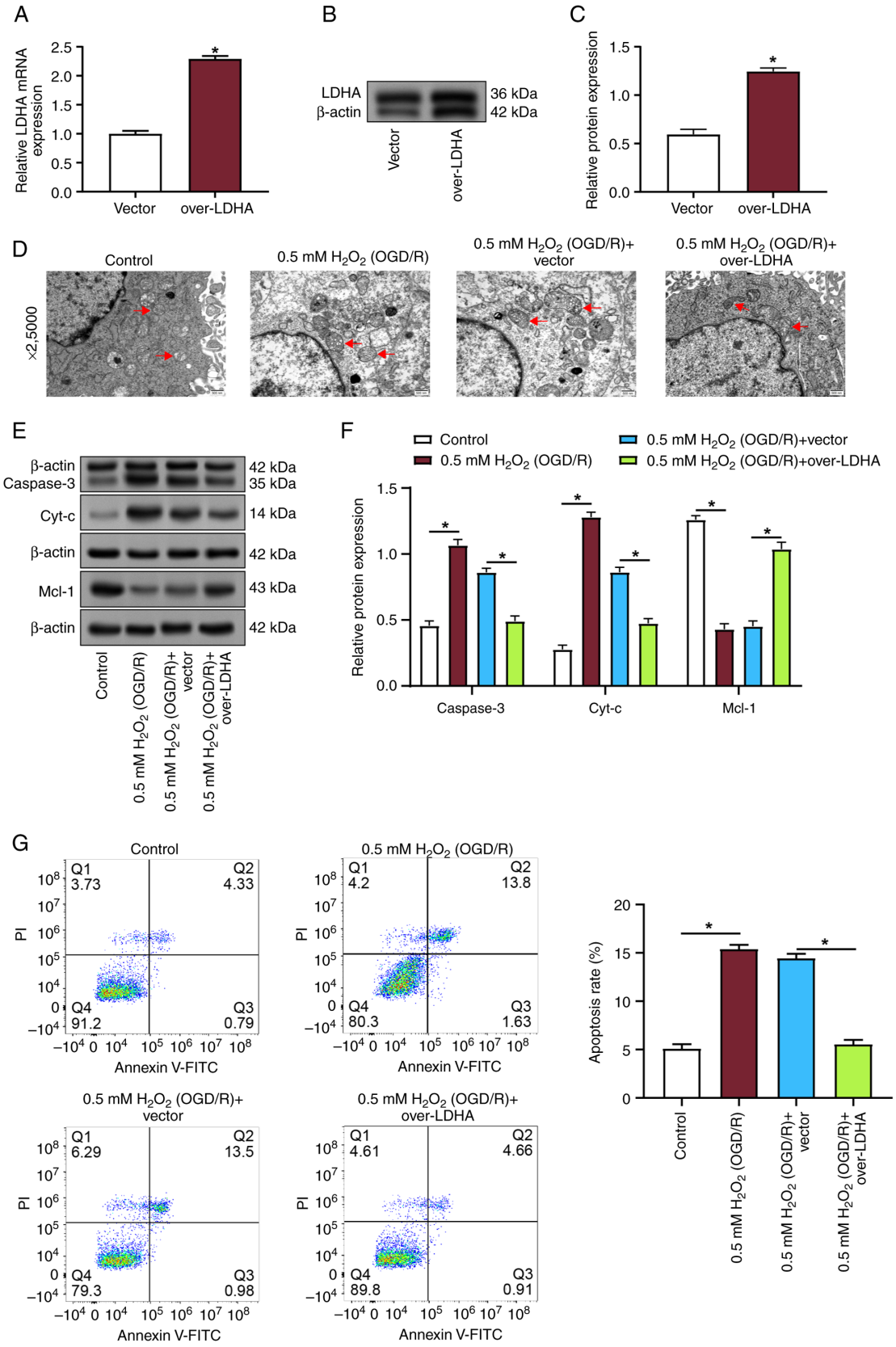

Figure 2. LDHA overexpression mitigates apoptosis and mitochondrial damage in OGD/R-treated VECs. (A) Reverse transcription-quantitative polymerase chain reaction analysis of LDHA mRNA in VECs transfected with vector or over-LDHA. (B) Representative western blot analysis of LDHA with β-actin as loading control. (C) Semi-quantification of LDHA protein expression relative to β-actin. (D) Transmission electron microscopy images of VECs at x2,500 magnification showing mitochondrial morphology. Red arrows indicate mitochondria (swollen and with disrupted cristae under OGD/R conditions). Scale bar: 500 nm. (E) Western blot analysis of caspase-3, Cyt-c and Mcl-1 in VECs from the indicated groups; β-actin was used as the loading control. (F) Densitometric semi-quantification of relative protein expression normalized to β-actin for caspase-3, Cyt-c and Mcl-1. (G) Flow cytometric analysis of the effects of LDHA overexpression on apoptosis levels in VECs subjected to H_2O_2 (OGD/R) treatment. Data are presented as the mean ± SD of three independent experiments. *P<0.05 vs. vector or as indicated. H_2O_2, hydrogen peroxide; OGD/R, oxygen-glucose deprivation/reperfusion; VECs, vascular endothelial cells; LDHA, lactate dehydrogenase A; WB, western blotting; PI, propidium iodide; FITC, fluorescein isothiocyanate; Cyt-c, cytochrome *c*.

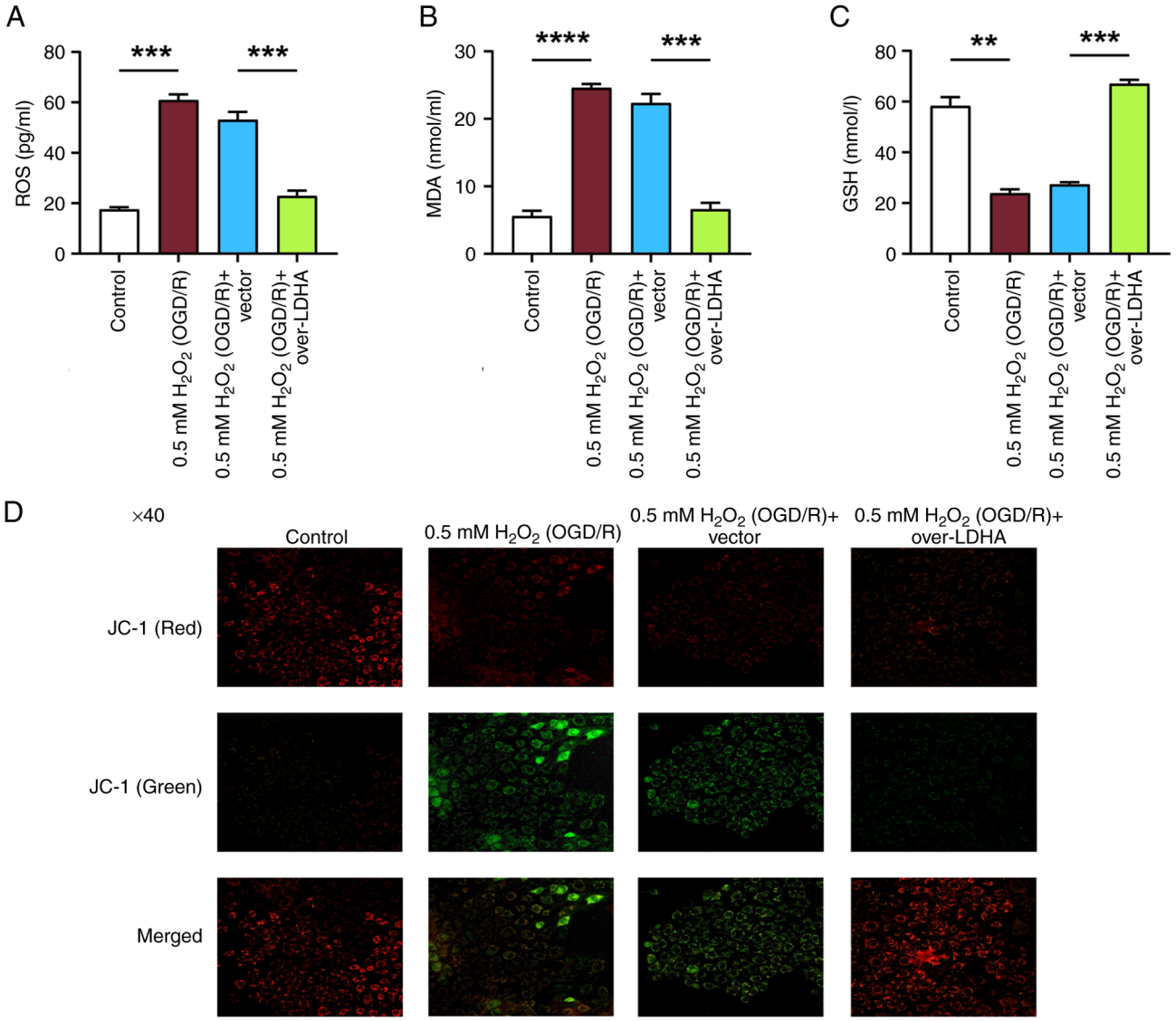

Figure 3. Effect of LDHA overexpression on oxidative stress markers and MMP in VECs under OGD/R conditions. Levels of (A) ROS, (B) MDA and (C) GSH in VECs following 0.5 mM H_2O_2 (OGD/R) treatment with or without LDHA overexpression. (D) MMP analysis using JC-1 fluorescent dye in VECs treated with 0.5 mM H_2O_2 (OGD/R) and overexpressing LDHA. Cells were assessed for red and green fluorescence, where red fluorescence indicates intact MMP and green fluorescence indicates depolarized MMP. Magnification, x40. Data are presented as the mean ± SD of three independent experiments. **P<0.01, ***P<0.001 and ****P<0.0001. H_2O_2, hydrogen peroxide; OGD/R, oxygen-glucose deprivation/reperfusion; VECs, vascular endothelial cells; LDHA, lactate dehydrogenase A; ROS, reactive oxygen species; MDA, malondialdehyde; GSH, glutathione; MMP, mitochondrial membrane potential.

further demonstrated that 0.5 mM H_2O_2 (OGD/R) treatment significantly promoted apoptosis in VECs; however, *LDHA* overexpression effectively mitigated the pro-apoptotic effects of oxidative stress (Fig. 2G). These findings indicated that upregulation of LDHA under oxidative stress conditions could alleviate OGD/R-induced apoptosis and mitochondrial damage in VECs.

LDHA overexpression reduces oxidative stress and preserves MMP in VECs under OGD/R conditions. To investigate the function of LDHA in oxidative stress, the levels of ROS, GSH and MDA were detected in VECs treated with 0.5 mM H_2O_2 (OGD/R) and overexpressing LDHA. Compared with those in the control group, 0.5 mM H_2O_2 (OGD/R) treatment resulted in significant increases in MDA and ROS, along with a reduction in GSH; however, LDHA overexpression reversed these effects, and restored MDA, ROS and GSH levels (Fig. 3A-C). MMP was next assessed using the JC-1 fluorescent dye. Control cells predominantly exhibited red fluorescence, indicating intact MMP (Fig. 3D). By contrast, 0.5 mM H_2O_2 (OGD/R)-treated cells showed a marked increase in green fluorescence, indicating mitochondrial depolarization. LDHA overexpression, however, resulted in a higher red/green fluorescence ratio in contrast to the two control groups and the 0.5 mM H_2O_2 (OGD/R) + vector group, suggesting that LDHA overexpression mitigated the loss of MMP induced by oxidative stress. Taken together, these results demonstrated that LDHA overexpression may reduce ROS generation and help maintain MMP during OGD/R-induced oxidative damage in VECs.

LDHA overexpression enhances HIF-1α expression and nuclear translocation in VECs under OGD/R conditions. In the OGD/R model, HIF-1α activity is essential for the

adaptation of cells to hypoxic conditions and for promoting cell survival. To further investigate the effects of 0.5 mM H_2O_2 (OGD/R) and LDHA overexpression on HIF-1α expression and localization in VECs, WB was employed. The outcomes indicated that compared with in the control group, the expression levels of total HIF-1α were increased in VECs treated with 0.5 mM H_2O_2 (OGD/R) (Fig. 4A and B). Moreover, LDHA overexpression further enhanced the expression of HIF-1α compared with that in the 0.5 mM H_2O_2 (OGD/R) + vector group. Further analysis revealed that both cytoplasmic and nuclear HIF-1α levels were elevated in the 0.5 mM H_2O_2 (OGD/R) group compared with in the control group (Fig. 4C-F). LDHA overexpression also promoted the accumulation of HIF-1α in both the cytoplasm and nucleus, compared with that in the 0.5 mM H_2O_2 (OGD/R) + vector group. IF staining was used to assess the cellular localization of HIF-1α. Under control conditions, HIF-1α was primarily localized in the cytoplasm (Fig. 4G). After 0.5 mM H_2O_2 (OGD/R) treatment, HIF-1α expression was markedly upregulated. Notably, HIF-1α expression was further elevated in VECs transfected with an LDHA overexpression plasmid following OGD/R. These findings suggested that LDHA upregulation may promote HIF-1α nuclear translocation in VECs under OGD/R conditions, potentially contributing to cellular adaptation and survival under oxidative stress.

LDHA alleviates OGD/R-induced VEC apoptosis and mitochondrial damage via HIF-1α nuclear translocation. To further explore the role of LDHA in apoptosis and mitochondrial damage, the effects of LDHA overexpression and the HIF-1α inhibitor (PX478) on VECs exposed to 0.5 mM H_2O_2 (OGD/R) were investigated by flow cytometry. The outcomes demonstrated that LDHA overexpression significantly suppressed apoptosis induced by 0.5 mM H_2O_2 (OGD/R) in VECs; however, treatment with PX478 reversed the protective effect of LDHA overexpression on apoptosis (Fig. 5A). A ROS assay kit was subsequently employed to quantify ROS levels. Compared with those in the 0.5 mM H_2O_2 (OGD/R) + vector group, LDHA overexpression resulted in a marked reduction in ROS levels (Fig. 5B). By contrast, treatment with PX478 diminished the effect of LDHA overexpression on ROS levels (Fig. 5B). The MMP was assessed using JC-1 fluorescent dye. In 0.5 mM H_2O_2 (OGD/R)-treated cells, green fluorescence was markedly enhanced, indicating mitochondrial depolarization (Fig. 5C). By contrast, LDHA overexpression improved the red/green fluorescence ratio, suggesting a preserved MMP; however, this effect was attenuated when PX478 was applied, indicating that the protective role of LDHA overexpression in MMP preservation was partially dependent on HIF-1α signaling. To directly assess the effect on HIF-1α expression, WB was performed to detect HIF-1α protein expression levels in the cytoplasm and nucleus under OGD/R conditions. LDHA overexpression significantly elevated HIF-1α expression in both compartments, whereas PX478 treatment led to a notable decrease in HIF-1α levels (Fig. 5D-G). These findings collectively suggested that LDHA overexpression could alleviate OGD/R-induced mitochondrial damage in VECs, likely through the promotion of HIF-1α nuclear translocation.

LDHA overexpression enhances glycolytic activity and modulates metabolic pathways in VECs under OGD/R conditions. Pyruvate, lactate and succinate serve important roles in cellular energy metabolism, directly affecting mitochondrial function and ATP synthesis (24). To further explore the impact of LDHA overexpression on cellular metabolism, the levels of pyruvate, lactate and succinate were measured in VECs treated with 0.5 mM H_2O_2 (OGD/R) and overexpressing LDHA. The results showed that LDHA overexpression increased pyruvate and lactate levels, while reducing succinate levels in VECs subjected to 0.5 mM H_2O_2 (OGD/R) (Fig. 6A-C). Subsequently, the expression levels of key glycolytic genes [hexokinase 2 (HK2), phosphoglucomutase 5 (PGM5), pyruvate kinase M (PKM) and LDHA] were assessed in VECs by RT-qPCR. The data revealed that LDHA overexpression significantly promoted the expression levels of HK2, PGM5, PKM and LDHA compared with those in the 0.5 mM H_2O_2 (OGD/R) + vector group, indicating enhanced glycolytic activity in VECs (Fig. 6D). Further analysis of tricarboxylic acid (TCA) cycle-related genes [oxoglutarate dehydrogenase (OGDH), dihydrolipoamide dehydrogenase (DLD) and succinyl-CoA synthetase β subunit (SUCLG2)] in VECs treated with 0.5 mM H_2O_2 (OGD/R) and overexpressing LDHA showed that LDHA overexpression suppressed the expression levels of OGDH and DLD, while increasing SUCLG2 expression compared with those in the 0.5 mM H_2O_2 (OGD/R) + vector group (Fig. 6E). ECAR was measured to assess the dynamic metabolic changes in VECs. Upon glucose addition, all groups showed a rapid increase in ECAR, confirming the activation of glycolysis (Fig. 6F). The 0.5 mM H_2O_2 (OGD/R) + LDHA overexpression group exhibited higher ECAR increase compared with that in the 0.5 mM H_2O_2 (OGD/R) + vector and 0.5 mM H_2O_2 (OGD/R) groups. Following Oligo treatment, all groups showed a marked ECAR peak, indicating enhanced glycolytic activity. Notably, the ECAR in the 0.5 mM H_2O_2 (OGD/R) + LDHA overexpression group was higher than that in the other groups, suggesting that LDHA overexpression strongly enhanced glycolysis. After the addition of the glycolysis inhibitor 2-DG, ECAR was significantly decreased in all groups, returning to baseline levels. These results collectively demonstrated that LDHA overexpression may enhance glucose metabolism in VECs, promoting glycolysis and modulating metabolic pathways following OGD/R-induced damage.

LDHA alleviates oxidative stress-induced mitochondrial damage via glycolytic reprogramming in VECs. To further investigate whether LDHA protects against oxidative stress-induced mitochondrial injury through glycolytic reprogramming, LDHA-overexpressing VECs we treated with or without the glycolysis inhibitor 2-DG under 0.5 mM H_2O_2 (OGD/R) conditions. WB showed that compared with LDHA overexpression alone, the addition of 2-DG markedly increased the expression levels of the mitochondrial apoptosis-related proteins caspase-3 and Cyt-c, while reducing the expression of the anti-apoptotic protein Mcl-1 (Fig. 7A-D). The current study further evaluated oxidative stress markers. Compared with LDHA overexpression alone, treatment with 2-DG significantly increased ROS and MDA levels, while GSH levels were decreased (Fig. 7E-G). These findings support that LDHA overexpression may mitigate oxidative stress-induced

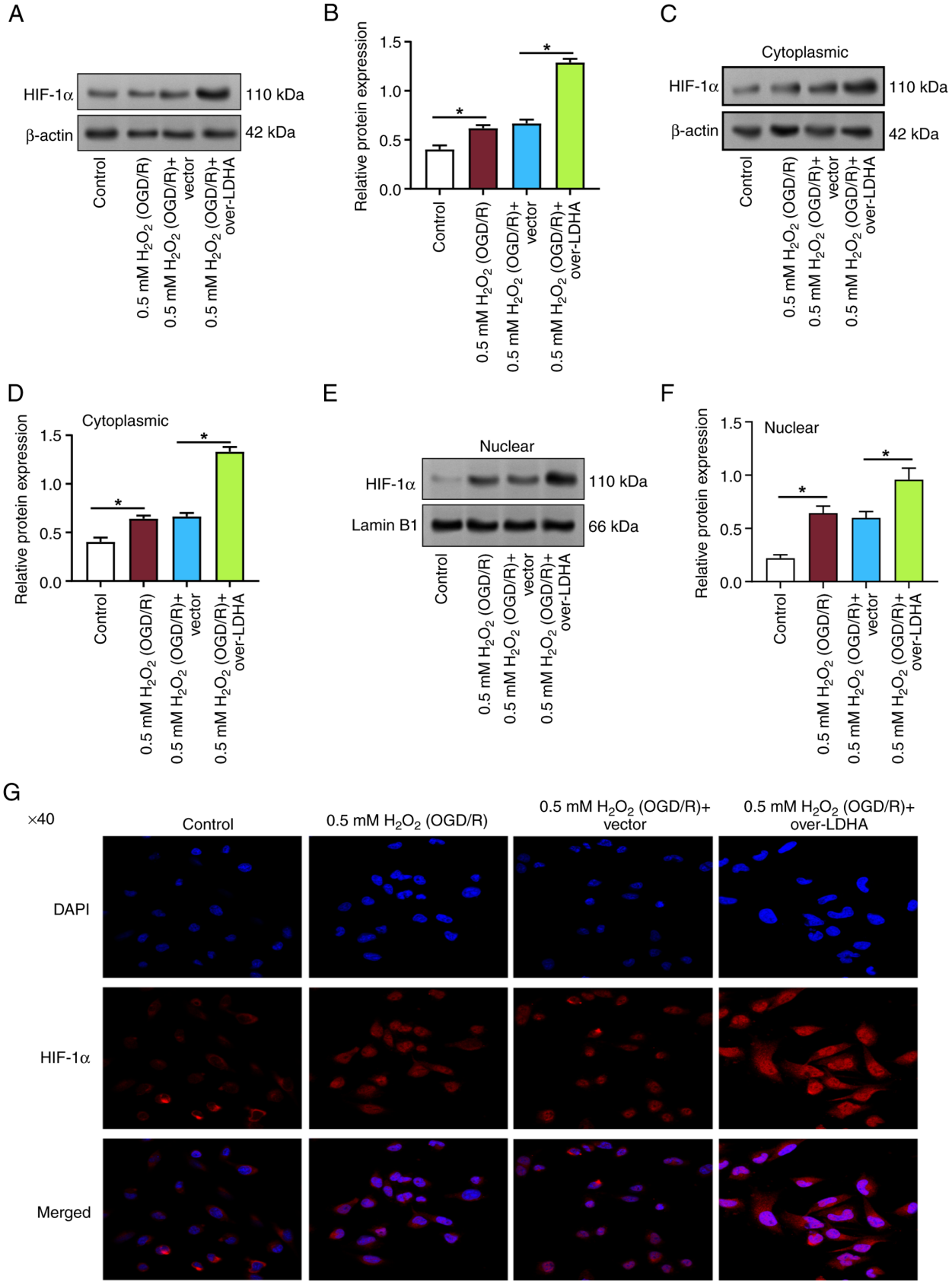

Figure 4. LDHA overexpression enhances HIF-1α expression and nuclear translocation in VECs under OGD/R conditions. (A) WB of total HIF-1α expression in VECs treated with 0.5 mM H_2O_2 (OGD/R) and overexpressing LDHA. (B) Semi-quantification of total HIF-1α protein levels from WB normalized to β-actin. (C) Representative western blot analysis of cytoplasmic HIF-1α from fractionated lysates; β-actin was used as the cytoplasmic control. (D) Semi-quantification of cytoplasmic HIF-1α protein in (C) using β-actin as a standard. (E) Representative western blot analysis of nuclear HIF-1α; Lamin B1 was used as a nuclear control. (F) Semi-quantification of nuclear HIF-1α protein in (E) using Lamin B1 as a standard. (G) Immunofluorescence staining of HIF-1α localization in VECs treated with 0.5 mM H_2O_2 (OGD/R) and overexpressing LDHA. Magnification, x40. Data are presented as the mean ± SD of three independent experiments. *P<0.05. H_2O_2, hydrogen peroxide; OGD/R, oxygen-glucose deprivation/reperfusion; VECs, vascular endothelial cells; LDHA, lactate dehydrogenase A; HIF-1α, hypoxia-inducible factor 1α; WB, western blotting.

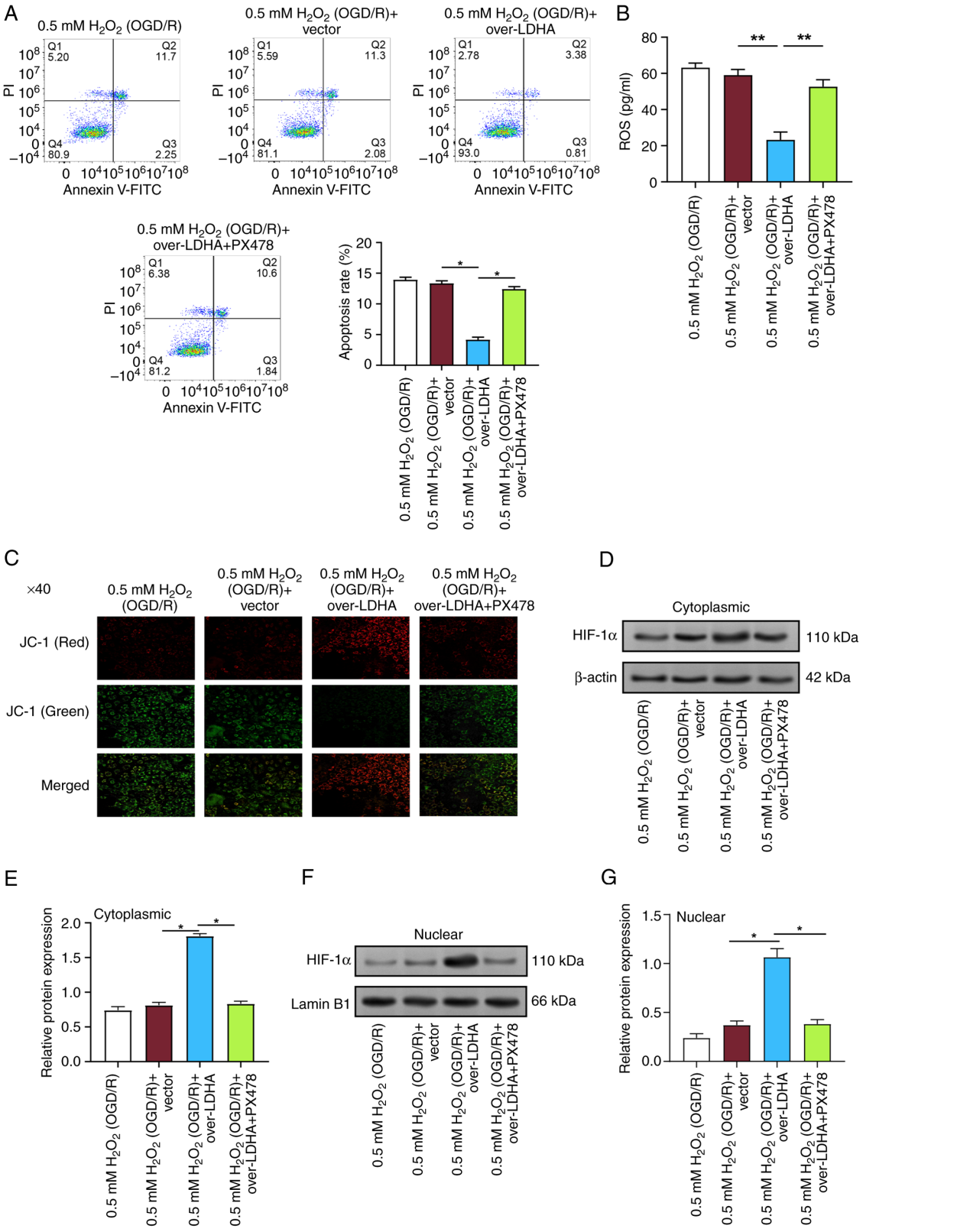

Figure 5. LDHA overexpression alleviates OGD/R-induced apoptosis and mitochondrial damage in VECs via HIF-1α nuclear translocation. (A) Flow cytometric analysis of apoptosis in VECs treated with 0.5 mM H_2O_2 (OGD/R) and overexpressing LDHA, with or without the HIF-1α inhibitor PX478. (B) ROS levels measured using a ROS assay kit in VECs treated with 0.5 mM H_2O_2 (OGD/R) and overexpressing LDHA, with or without PX478. (C) MMP was assessed by JC-1 fluorescent dye in VECs treated with 0.5 mM H_2O_2 (OGD/R) and overexpressing LDHA, with or without PX478. The images show representative red (intact MMP) and green (depolarized MMP) fluorescence. Magnification, x40. (D-G) WB of cytoplasmic and nuclear HIF-1α expression in VECs treated with 0.5 mM H_2O_2 (OGD/R) and overexpressing LDHA, with or without PX478. (D) Representative cytoplasmic HIF-1α western blot analysis; β-actin was used as a cytoplasmic control. (E) Semi-quantification of cytoplasmic HIF-1α in (D), normalized to β-actin. (F) Representative nuclear HIF-1α western blot analysis; Lamin B1 was used as a nuclear control. (G) Semi-quantification of nuclear HIF-1α in (F), normalized to Lamin B1. Data are presented as the mean ± SD of three independent experiments. *P<0.05 and **P<0.01. H_2O_2, hydrogen peroxide; OGD/R, oxygen-glucose deprivation/reperfusion; VECs, vascular endothelial cells; WB, western blotting; PI, propidium iodide; FITC, fluorescein isothiocyanate; LDHA, lactate dehydrogenase A; HIF-1α, hypoxia-inducible factor 1α; ROS, reactive oxygen species; MMP, mitochondrial membrane potential.

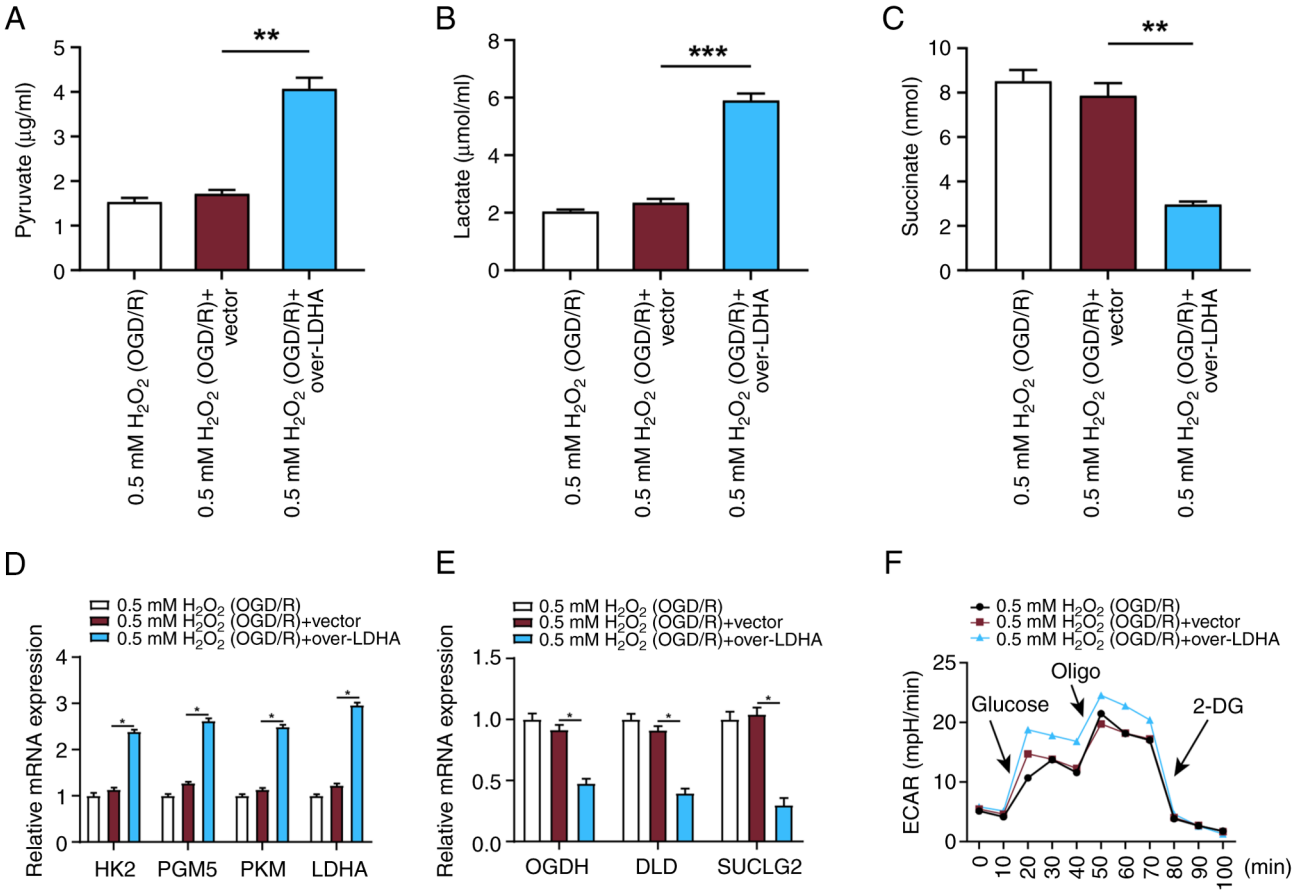

Figure 6. LDHA overexpression enhances glycolytic activity and modulates metabolic pathways in VECs under OGD/R conditions. (A) Pyruvate, (B) lactate and (C) succinate levels measured in VECs treated with 0.5 mM H_2O_2 (OGD/R) and overexpressing LDHA. (D) Expression levels of key glycolytic genes (HK2, PGM5, PKM and LDHA) were assessed by RT-qPCR in VECs treated with 0.5 mM H_2O_2 (OGD/R) and overexpressing LDHA. (E) Expression levels of tricarboxylic acid cycle-related genes (OGDH, DLD and SUCLG2) were assessed by RT-qPCR in VECs treated with 0.5 mM H_2O_2 (OGD/R) and overexpressing LDHA. (F) ECAR was measured to assess metabolic changes in VECs. Data are presented as the mean ± SD of three independent experiments. *P<0.05, **P<0.01 and ***P<0.001. H_2O_2, hydrogen peroxide; OGD/R, oxygen-glucose deprivation/reperfusion; VECs, vascular endothelial cells; LDHA, lactate dehydrogenase A; HK2, hexokinase 2; PGM5, phosphoglucomutase 5; PKM, pyruvate kinase M; OGDH, oxoglutarate dehydrogenase; DLD, dihydrolipoamide dehydrogenase; SUCLG2, succinate-CoA ligase β subunit; ECAR, extracellular acidification rate; Oligo, oligomycin; 2-DG, 2-deoxy-D-glucose; RT-qPCR, reverse transcription-quantitative polymerase chain reaction.

mitochondrial damage in VECs, likely through enhancing glycolysis and maintaining redox homeostasis.

LDHA overexpression induces lactic acid production without causing acidosis in VECs. A previous study demonstrated that in response to LDHA knockdown, lactate levels are increased (16). This has been attributed to the compensatory upregulation of LDHB activity under disease conditions, which may still drive lactate accumulation. Subsequently, the potential effects of LDHA overexpression on intracellular Na^+ and Ca^{2+} homeostasis were assessed. WB of transmembrane transporter proteins (NHE1 and NCX1) revealed no significant changes in their expression levels following LDHA overexpression under 0.5 mM H_2O_2 (OGD/R) conditions (Fig. 8A and B). Similarly, calcium assay measurements showed no significant alterations in intracellular Ca^{2+} concentration following LDHA overexpression (Fig. 8C). In addition, the expression levels of the lactate transporter MCT4 were examined by WB. The results indicated that LDHA overexpression upregulated MCT4 protein levels (Fig. 8D and E). Collectively, these data demonstrated that LDHA overexpression may increase lactate production in VECs without intracellular acidosis, as evidenced by unchanged NHE1/NCX1 expression and cytosolic Ca^{2+} together with upregulated MCT4 indicating enhanced lactate efflux.

LDHA overexpression enhances antioxidant defense and maintains redox balance in VECs under OGD/R conditions. To further explore the mechanism by which LDHA overexpression strengthens antioxidant defense and maintains redox balance, the levels of NAD^+ and NADH were measured in VECs treated with 0.5 mM H_2O_2 (OGD/R) and overexpressing LDHA. Using the NAD^+/NADH assay kit, it was revealed that LDHA overexpression reduced both NAD^+ and NADH levels in VECs subjected to OGD/R-induced damage (Fig. 9A and B). It has previously been shown that NADH interacts with LDHA to generate electrons, which could promote ROS production (25). Therefore, the reduction of ROS observed in the current study may be due to the decreased interaction between NADH and LDHA following overexpression. To investigate whether LDHA overexpression influences the activation of the pentose phosphate pathway (PPP) during OGD/R damage, NADPH levels and G6PDH activity were assessed in VECs. The results revealed that

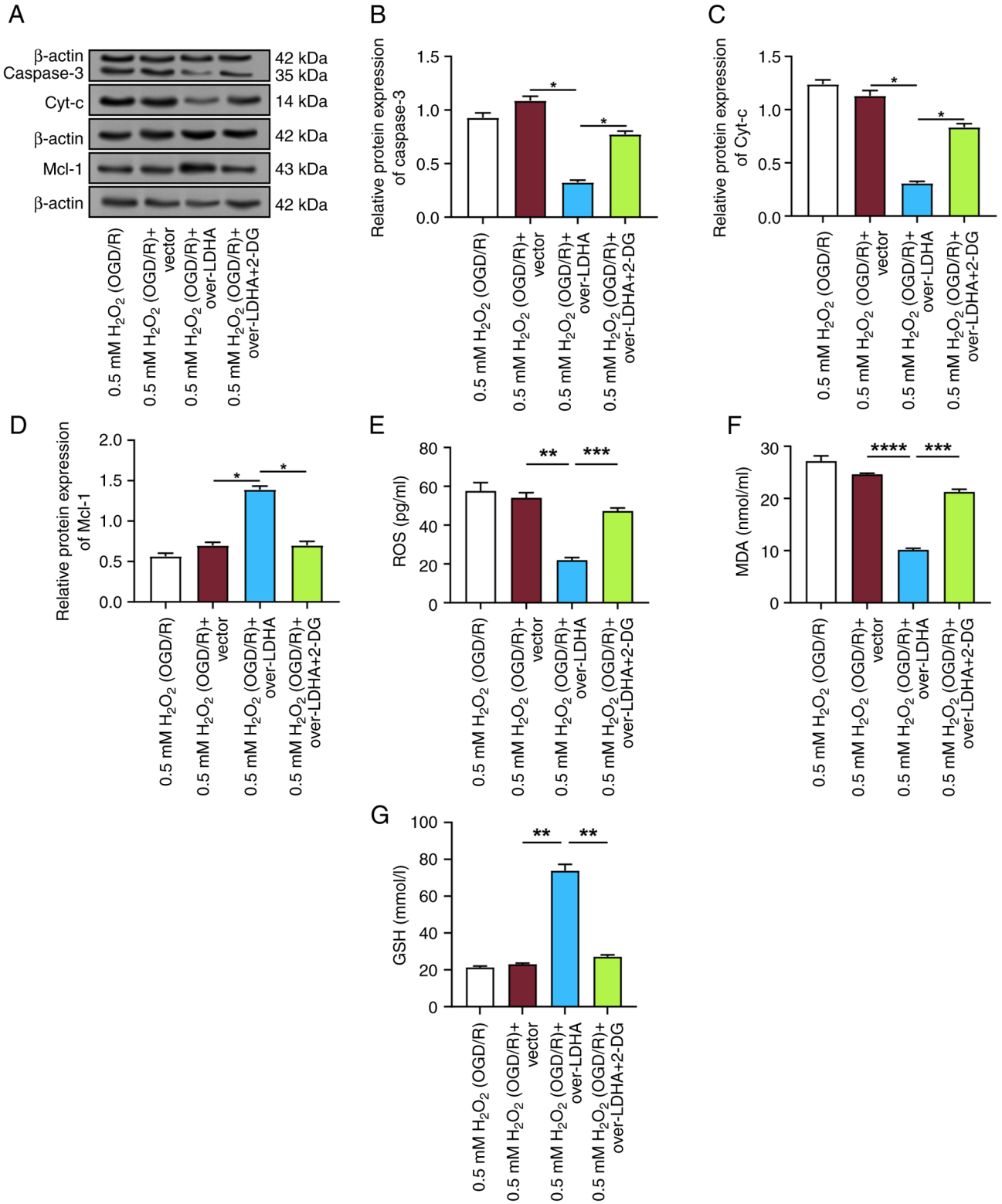

Figure 7. LDHA protects against oxidative stress-induced mitochondrial damage through glycolytic reprogramming in VECs. (A) Representative WB images of caspase-3, Cyt-c and Mcl-1 protein expression in VECs treated with 0.5 mM H_2O_2 (OGD/R) and overexpressing LDHA, with or without 2-DG. Semi-quantification of (B) caspase-3, (C) Cyt-c and (D) Mcl-1 protein levels normalized to internal controls. Measurement of (E) ROS, (F) MDA and (G) GSH levels in each group. Data are presented as the mean ± SD from three independent experiments. *P<0.05, **P<0.01, ***P<0.001 and ****P<0.0001. H_2O_2, hydrogen peroxide; OGD/R, oxygen-glucose deprivation/reperfusion; VECs, vascular endothelial cells; LDHA, lactate dehydrogenase A; 2-DG, 2-deoxy-D-glucose; WB, western blotting; ROS, reactive oxygen species; MDA, malondialdehyde; GSH, glutathione; Cyt-c, cytochrome *c*.

LDHA overexpression significantly increased both NADPH levels and G6PDH activity compared with those in the 0.5 mM H_2O_2 (OGD/R) + vector group (Fig. 9C and D). These outcomes indicated that LDHA overexpression may enhance activation of the PPP in VECs during oxidative stress induced by OGD/R.

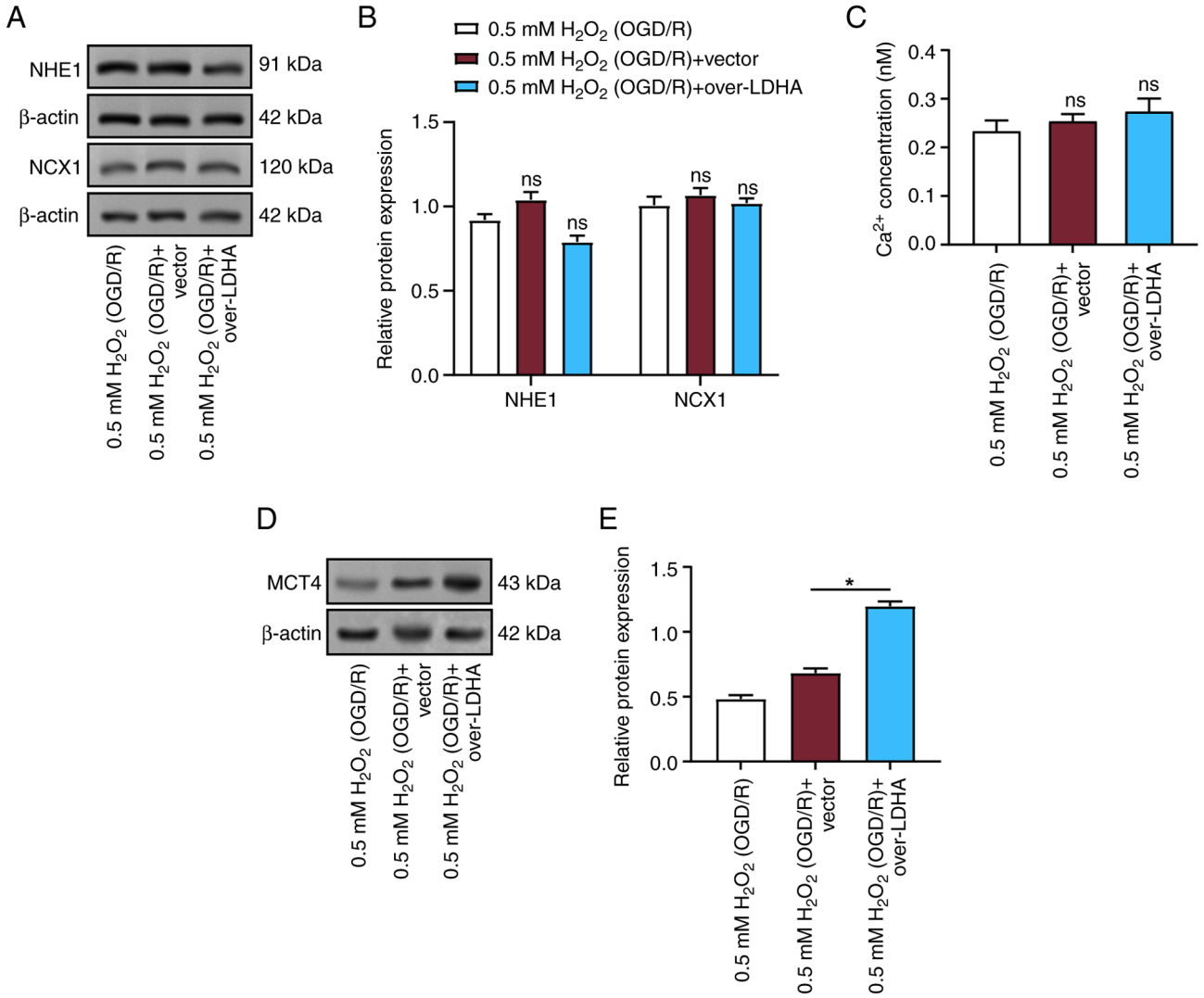

Figure 8. LDHA overexpression induces lactic acid production without causing acidosis in VECs. (A) Representative WB showing protein levels of NHE1 and NCX1 in VECs treated with 0.5 mM H_2O_2 (OGD/R), 0.5 mM H_2O_2 (OGD/R) + vector, or 0.5 mM H_2O_2 (OGD/R) + LDHA overexpression. (B) Semi-quantification of NHE1 and NCX1 protein expression. (C) Intracellular Ca^{2+} concentration measured in VECs after LDHA overexpression under 0.5 mM H_2O_2 (OGD/R) conditions. (D) WB of MCT4 expression in VECs after LDHA overexpression under 0.5 mM H_2O_2 (OGD/R) conditions. (E) Semi-quantification of MCT4 protein expression in VECs treated with 0.5 mM H_2O_2 (OGD/R) and overexpressing LDHA. Data are presented as the mean ± SD of three independent experiments. *P<0.05; ns, not significant. H_2O_2, hydrogen peroxide; OGD/R, oxygen-glucose deprivation/reperfusion; VECs, vascular endothelial cells; LDHA, lactate dehydrogenase A; NHE1, sodium-proton exchanger 1; NCX1, sodium-calcium exchanger 1; MCT4, monocarboxylate transporter 4; WB, western blotting.

Discussion

Endothelial cells are essential for the progression and formation of aneurysms through mechanisms such as maintaining vascular integrity, regulating vasomotion and participating in inflammatory responses (26). Morel *et al* (27) reported that both low and excessively high WSS in CAs can alter endothelial cell morphology. Low WSS was shown to downregulate cytoskeletal proteins and upregulate extracellular matrix proteins, whereas extremely high WSS induced the opposite effects. These changes may contribute to vascular remodeling in aneurysms. Additionally, Zhu *et al* (28) indicated that high mobility group box 1 (HMGB1) can induce oxidative stress and inflammation in endothelial cells exposed to WSS, whereas HMGB1 knockdown can attenuate this process. During apoptosis, Cyt-c is typically released from mitochondria into the cytoplasm when mitochondrial membrane permeability increases. It then binds with Apaf-1 to form apoptosomes. By blocking the permeability of the outer membrane of the mitochondria and stopping the release of Cyt-c, Mcl-1 can alter the susceptibility of the cell to apoptotic signals (29). Huang *et al* (30) noted that FOXO1 reduces Mcl-1 expression by suppressing its transcription, thereby promoting apoptosis, inflammation and inhibition of cell proliferation in human brain vascular smooth muscle cells. The current study observed significant apoptosis in VECs following treatment with 0.5 mM H_2O_2 (OGD/R), alongside increased expression levels of apoptosis-related proteins, including caspase-3, caspase-9 and caspase-8. Additionally, mitochondrial pathway-related proteins were affected, with elevated Cyt-c expression and decreased levels of Mcl-1 detected following treatment with 0.5 mM H_2O_2 (OGD/R), indicating that oxidative stress can promote VEC apoptosis by activating the mitochondrial apoptotic pathway.

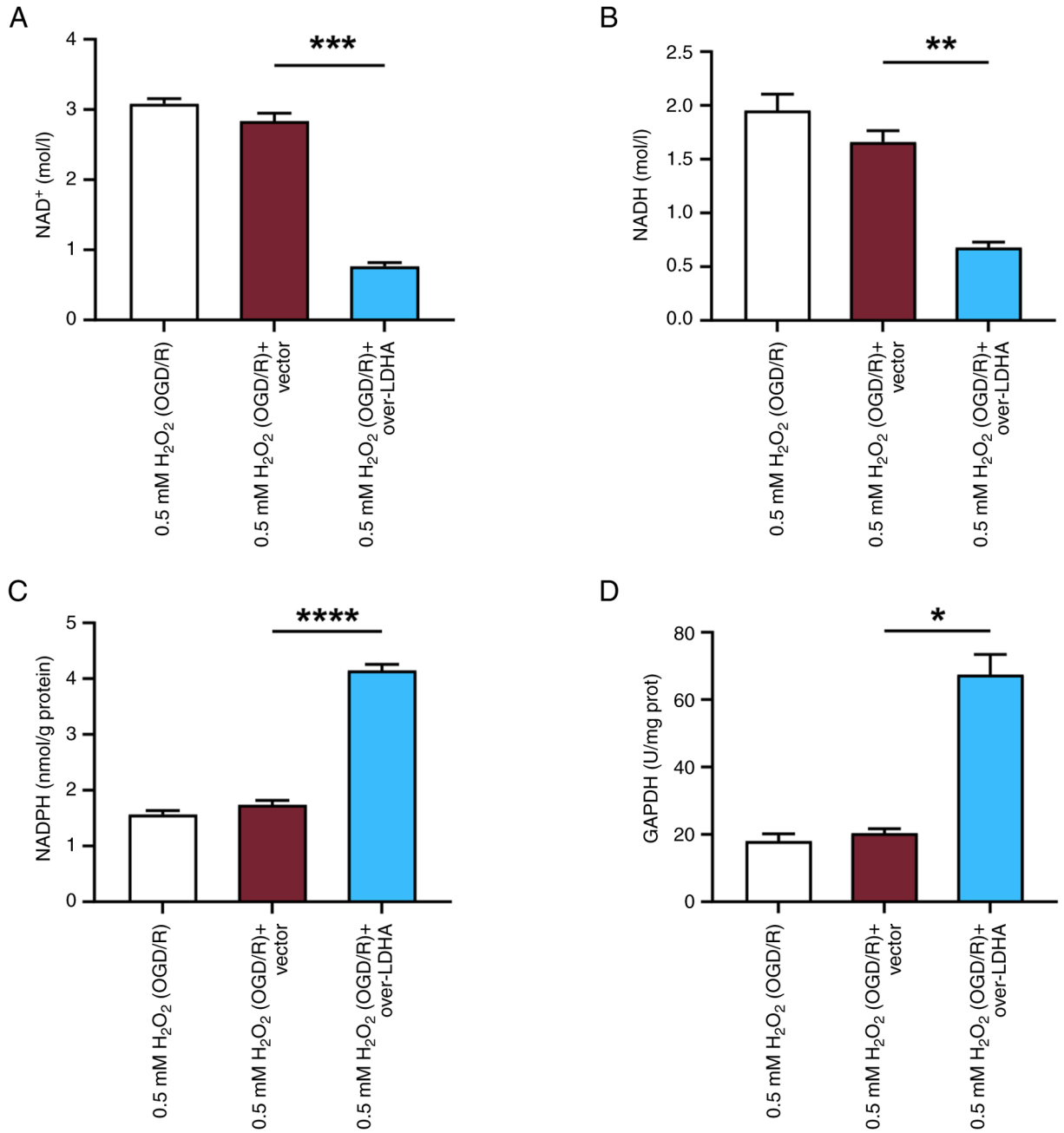

Figure 9. LDHA overexpression enhances antioxidant defense and maintains redox balance in VECs under OGD/R conditions. (A) NAD^+, (B) NADH and (C) NADPH levels, and (D) G6PDH activity in VECs treated with 0.5 mM H_2O_2 (OGD/R) and overexpressing LDHA. Data are presented as the mean ± SD of three independent experiments. $^*P<0.05$, $^{**}P<0.01$, $^{***}P<0.001$ and $^{****}P<0.0001$ vs 0.5 mM H_2O_2 (OGD/R) + vector group. H_2O_2, hydrogen peroxide; OGD/R, oxygen-glucose deprivation/reperfusion; VECs, vascular endothelial cells; LDHA, lactate dehydrogenase A; G6PDH, glucose-6-phosphate dehydrogenase.

Oxidative stress-induced ROS can oxidize lipids, leading to mitochondrial membrane damage (31). This damage disrupts mitochondrial permeability, causes a loss of membrane potential, and subsequently impairs ATP synthesis. Mitochondrial damage will aggravate oxidative stress, forming a vicious cycle. Tavris *et al* (32) revealed that vascular smooth muscle cells in abdominal aortic aneurysms exhibit mitochondrial dysfunction and increased oxidative stress, leading to abnormal mitochondrial morphology, enhanced ROS production, weakened antioxidant responses and aggravated DNA damage. Nguyen *et al* (33) investigated the function of mitochondrial oxidative stress in various types of brain injuries, both traumatic and non-traumatic. This previous study highlighted the reliance of the brain on mitochondrial function to meet its oxidative demands. However, the effects of ROS varied across different injury types. Chen *et al* (34) emphasized the critical function of mitochondrial dysfunction and necrotic apoptosis in the formation of CAs. This previous study observed upregulation of these processes in monocytes/macrophages and vascular smooth muscle cells, suggesting potential new targets for the diagnosis and treatment of IAs. The current study discovered that LDHA overexpression alleviated apoptosis and mitochondrial damage induced by oxidative stress in VECs. Specifically, LDHA overexpression improved mitochondrial morphology, reduced swelling and damage, and suppressed the upregulation of caspase-3 and Cyt-c, while restoring Mcl-1

expression. Additionally, LDHA overexpression significantly reduced ROS and MDA levels, restored GSH levels and protected MMP from oxidative stress-induced damage. These outcomes imply that LDHA overexpression has a protective function in mitigating oxidative stress and mitochondrial dysfunction in VECs.

In response to OGD/R, the levels of the essential transcription factor HIF-1 are typically increased (35). HIF-1α and HIF-1β are the two subunits that make up HIF-1 (36). Under hypoxic conditions, HIF-1α degradation is inhibited, resulting in increased stability and accumulation within the cell. The accumulation of HIF-1α enables its dimerization with HIF-1β to form an active HIF-1 complex. This complex translocates to the nucleus and activates the expression of several target genes (37). Kalashnyk *et al* (38) reported that α7 nicotinic acetylcholine receptors are upregulated in hepatocytes and U373 cells (human glioblastoma/astrocytoma cell line). These receptors interact with HIF-1α and influence its translocation, particularly under hypoxic conditions. Papandreou *et al* (39) reported that HIF-1 induces pyruvate dehydrogenase kinase 1 (PDK1), which suppresses mitochondrial function and reduces mitochondrial oxygen consumption. Although HIF-1 promotes glycolysis, it paradoxically inhibits mitochondrial oxygen utilization. This inhibition of oxygen utilization paradoxically increases intracellular oxygen tension, thereby reducing cell death in hypoxic environments. Han *et al* (40) demonstrated that Axl promotes M1 macrophage polarization through the STAT1/HIF-1α signaling pathway; by contrast, inhibiting Axl can reduce M1 macrophage infiltration and prevent IA rupture. PX478, as an inhibitor targeting HIF-1α, can effectively block HIF-1α-mediated transcriptional activation by altering the stability of HIF-1α. In the present study, overexpression of LDHA under OGD/R conditions enhanced the expression and nuclear translocation of HIF-1α, helping VECs adapt to the hypoxic environment and improving cell survival. Furthermore, LDHA overexpression mitigated OGD/R-induced cell apoptosis and mitochondrial damage, whereas treatment with the HIF-1α inhibitor PX478 reversed the protective effects of LDHA overexpression. These findings indicated that LDHA may exert its protective role through the HIF-1α signaling pathway by alleviating oxidative stress-induced mitochondrial damage and apoptosis.

In the brain, glucose serves as the main oxidative substrate for energy synthesis. Energy dysregulation may be indicated by mitochondrial injury, which would impact glucose metabolism. Gusdon *et al* (41) reported that after aSAH, patients exhibit a shift in metabolism toward glycolysis, characterized by elevated levels of glycolytic metabolites and reduced levels of oxidative metabolites. Dai *et al* (42) highlighted the function of LDHA in T-cell energy metabolism, emphasizing its crucial involvement in glycolysis. Specifically, LDHA was shown to promote lactate production, exhibit non-classical enzymatic activity and contribute to oxidative stress in immune-related diseases, such as *Listeria monocytogenes* and murine cytomegalovirus infections. Tian *et al* (43) discovered that VGLL4 can alleviate neurodegeneration in models of Alzheimer's disease (AD), including AD model mice and AD model cells, by upregulating LDHA expression and enhancing lactate production. NHE1 and NCX1 are two distinct transmembrane transporters that serve key roles in cellular ion homeostasis and signal transduction. Yin *et al* (44) showed that limonene protects against endothelial dysfunction in type 2 diabetes by inhibiting the TRPM2/NHE1 signaling pathway, reducing oxidative stress and mitigating mitochondrial damage. Glycolysis generates energy by breaking down glucose, whereas the TCA cycle produces a greater amount of ATP through a more complete oxidative process. The present study demonstrated that LDHA overexpression enhanced pyruvate and lactate levels, while reducing succinate levels. These findings suggested a potential inhibition of mitochondrial function. In addition, LDHA overexpression significantly promoted the expression of glycolytic genes and enhanced glycolytic activity, while suppressing the expression of TCA cycle-related genes. After LDHA-overexpressing cells were treated with 2-DG, the expression of mitochondrial apoptosis-related proteins caspase3 and Cyt-c was increased, whereas the expression of Mcl-1 was decreased. Furthermore, ROS and MDA levels were elevated, and GSH levels were reduced. These findings further suggested that LDHA may protect mitochondria from oxidative stress-induced endothelial cell injury through glycolytic reprogramming. Although lactate levels increased following LDHA overexpression, no acidosis was observed, and there were no significant changes in Na^+ and Ca^{2+} homeostasis or transporter expression. In addition, LDHA overexpression upregulated the lactate transporter MCT4, which may help alleviate lactate accumulation.

During cellular respiration, NAD^+ and NADH serve crucial roles. Metabolic processes such as glycolysis, the TCA cycle and oxidative phosphorylation all depend on the exchange between NAD^+ and NADH (45). Zhao *et al* (46) demonstrated that NAD^+ activates the sirtuin 1/peroxisome proliferator-activated receptor γ coactivator 1α pathway. This activation was shown to improve cognitive function in rats with chronic cerebral ischemia, suppress neuroinflammation, protect mitochondria and reduce ROS production. Lee *et al* (47) revealed that supplements enhancing the NAD/NADH ratio and mitochondrial function can provide protection to brain endothelial cells against oxidative stress induced by OGD. These supplements also improved tight junction protein expression and alleviated damage in a mouse model of intracerebral hemorrhage. The PPP is an important cellular metabolic pathway; while similar to glycolysis, the PPP serves a different primary function. Zhang *et al* (48) conducted a bioinformatics analysis to identify four oxidative stress-related diagnostic biomarkers (FLVCR2, SDSL, TBC1D2, SLC31A1). This previous study demonstrated that these biomarkers were associated with oxidative stress, ROS accumulation, abnormal glucose metabolism and immune suppression infiltration in IAs. These findings provide new insights for clinical management. G6PDH is a key enzyme in the PPP, catalyzing the transformation of G6P to 6-phosphoglucono-δ-lactone, accompanied by the production of NADPH. Studies have shown that G6PD deficiency reduces NADPH levels in microglia, triggering oxidative stress and functional damage. Supplementation with metabolites and small molecules has been shown to increase NADPH production and improve microglial function (49,50). Wiśniewski *et al* (51) noted that, after aSAH, individuals with delayed cerebral ischemia (DCI) exhibited higher F2-isoprostane (IsoP) levels and lower G6PD levels. Both changes were associated with the occurrence and prognosis

of DCI. Reduced G6PD may impair antioxidant responses and elevate F2-IsoP levels. In the present study, overexpression of LDHA in VECs subjected to OGD/R treatment led to a decrease in NAD^+ and NADH levels. It also reduced ROS generation, while increasing NADPH levels and G6PDH activity. This could enhance the activity of the PPP, thereby improving the cellular antioxidant defense capacity.

HIF-1α is a pivotal transcription factor that orchestrates cellular responses to hypoxia and oxidative stress. The current study demonstrated that LDHA overexpression enhanced HIF-1α expression and nuclear translocation of HIF-1α. However, the mechanisms by which LDHA affects the downstream targets of HIF-1α to protect blood vessels remain to be investigated. Notably, HIF-1α upregulates VEGF, a key angiogenic factor that promotes endothelial cell survival, proliferation and migration, thereby maintaining vascular integrity and reducing aneurysm progression risk (52,53). In addition, HIF-1α induces the expression of PDK1, which redirects pyruvate metabolism towards lactate production, enhances glycolytic activity and reduces mitochondrial ROS generation (54). This metabolic reprogramming supports energy homeostasis and mitigates oxidative injury under hypoxic stress. Furthermore, HIF-1α modulates the balance of Bcl-2 family proteins by upregulating anti-apoptotic proteins, such as Bcl-2 and Bcl-xL, while downregulating pro-apoptotic Bax, thus protecting VECs from oxidative stress-induced apoptosis (55). HIF-1α also induces antioxidant enzymes, such as superoxide dismutase and catalase, neutralizes ROS and upregulates MCT4, facilitating lactate efflux and preventing acidosis, maintaining cellular pH homeostasis (56). Collectively, these downstream targets contribute to the protective effects observed in VECs under oxidative stress. By promoting glycolysis, enhancing angiogenesis, inhibiting apoptosis and improving antioxidant defenses, HIF-1α may have a central role in maintaining vascular integrity and preventing CA progression. Future research should further elucidate the interactions between LDHA and HIF-1α, as well as their downstream proteins, to develop targeted interventions for CAs and related vascular disorders.

The present study demonstrated that LDHA overexpression promoted the activation and nuclear translocation of HIF-1α, which is known to regulate downstream pathways involved in metabolic reprogramming and vascular protection. Consistent with this, it was observed that LDHA overexpression enhanced the expression of glycolytic enzymes, such as HK2, PGM5 and PKM, increased the expression of the lactate transporter MCT4, elevated NADPH production and enhanced G6PDH activity. Although the current data suggested that HIF-1α activation may contribute to these changes, the direct regulatory relationships between HIF-1α and these downstream proteins require further experimental validation.

In conclusion, the outcomes of the current study present compelling evidence suggesting that LDHA overexpression mitigates oxidative stress-induced apoptosis and mitochondrial damage in VECs under OGD/R conditions. By enhancing glycolytic activity and promoting the nuclear translocation of HIF-1α, LDHA could contribute to cellular adaptation and survival under oxidative stress conditions. Furthermore, LDHA overexpression may activate the PPP, boosting antioxidant defense and maintaining redox balance. These effects collectively support the notion that LDHA serves a protective role in VECs under oxidative damage, potentially offering a novel therapeutic target for conditions such as ischemic stroke and aSAH, where mitochondrial dysfunction and oxidative stress are central to pathogenesis.

Acknowledgements

Not applicable.

Funding

This work was supported by the Songjiang District Science and Technology Key Project (grant no. 2025SJKJGG085).

Availability of data and materials

The data generated in the present study may be requested from the corresponding author.

Authors' contributions

BD, LY, AY and YZ conceived and designed the research. BD and LY performed the experiments and acquired the data, analyzed and interpreted the data, and drafted the manuscript. BD performed statistical analysis. AY and YZ revised the manuscript for important intellectual content. BD and LY confirm the authenticity of all the raw data. All authors read and approved the final manuscript.

Ethics approval and consent to participate

Not applicable.

Patient consent for publication

Not applicable.

Competing interests

The authors declare that they have no competing interests.

References

1. Abbate PM, Hasan AH, Venier A, Vauclin V, Pizzuto S, Sgreccia A, Di Maria F, Coskun O, Mizutani K, Rodesch G and Consoli: The cerebral arterial wall in the development and growth of intracranial aneurysms. App Sci 12: 5964, 2022.
2. Tawk RG, Hasan TF, D'Souza CE, Peel JB and Freeman WD: Diagnosis and treatment of unruptured intracranial aneurysms and aneurysmal subarachnoid hemorrhage. Mayo Clinic Proceedings, Elsevier, 2021.
3. Weiland J, Beez A, Westermaier T, Kunze E, Sirén AL and Lilla N: Neuroprotective strategies in aneurysmal subarachnoid hemorrhage (aSAH). Int J Mol Sci 22: 5442, 2021.
4. Allaw S, Khabaz K, Given TC, Montas DM, Alcazar-Felix RJ, Srinath A, Kass-Hout T, Carroll TJ, Hurley MC and Polster SP: A review of intracranial aneurysm imaging modalities, from CT to state-of-the-art MR. Am J Neuroradiol 46: 1082-1092, 2025.
5. Sahlein DH, Gibson D, Scott JA, DeNardo A, Amuluru K, Payner T, Rosenbaum-Halevi D and Kulwin C: Artificial intelligence aneurysm measurement tool finds growth in all aneurysms that ruptured during conservative management. J Neurointerv Surg 15: 766-770, 2023.

6. de Liyis BG, Surya SC and Tini K: Effectivity and safety of endovascular coiling versus microsurgical clipping for aneurysmal subarachnoid hemorrhage: A systematic review and meta-analysis. Clin Neurol Neurosurg 236: 108058, 2024.
7. Huang X, Wang Z, Shen Z, Lei F, Liu YM, Chen Z, Qin JJ, Liu H, Ji YX, Zhang P, *et al*: Projection of global burden and risk factors for aortic aneurysm-timely warning for greater emphasis on managing blood pressure. Ann Med 54: 553-564, 2022.
8. Salnikova D, Orekhova V, Grechko A, Starodubova A, Bezsonov E, Popkova T and Orekhov A: Mitochondrial dysfunction in vascular wall cells and its role in atherosclerosis. Int J Mol Sc 22: 8990, 2021.
9. Wang Z, Ma J, Yue H, Zhang Z, Fang F, Wang G, Liu X and Shen Y: Vascular smooth muscle cells in intracranial aneurysms. Microvasc Res 149: 104554, 2023.
10. Kaur MM and Sharma S: Mitochondrial repair as potential pharmacological target in cerebral ischemia. Mitochondrion 63: 23-31, 2022.
11. Zhao W, Zhang H and Su JY: MicroRNA-29a contributes to intracranial aneurysm by regulating the mitochondrial apoptotic pathway. Mol Med Rep 18: 2945-2954, 2018.
12. Wang S, Wang J, Niu Z, Zhang K, Yang T, Hou S and Lin N: Causal relationship between mitochondrial-associated proteins and cerebral aneurysms: A Mendelian randomization study. Front Neurol 15: 1405086, 2024.
13. Lin Y, Wang Y and Li PF: Mutual regulation of lactate dehydrogenase and redox robustness. Front Physiol 13: 1038421, 2022.
14. Wang G, Liu S, Kong X, Jiao H, Tong F, Guo Z, Zhang M, Guan X, Ren N, Li W, *et al*: Lipocalin-2 induced LDHA expression promotes vascular remodelling in pulmonary hypertension. Cell Prolif 57: e13717, 2024.
15. Wu D, Wang S, Wang F, Zhang Q, Zhang Z and Li X: Lactate dehydrogenase A (LDHA)-mediated lactate generation promotes pulmonary vascular remodeling in pulmonary hypertension. J Transl Med 22: 738, 2024.
16. Wu J, Lu L, Dai B and Yu A: Unraveling the role of LDHA and VEGFA in oxidative stress: A pathway to therapeutic interventions in cerebral aneurysms. Biomol Biomed 25: 360-374, 2025.
17. Renu K, Gopalakrishnan AV and Madhyastha H: Is periodontitis triggering an inflammatory response in the liver, and does this reaction entail oxidative stress? Odontology 113: 889-902, 2025.
18. Fang L, Yu Z, Qian X, Fang H and Wang Y: LDHA exacerbates myocardial ischemia-reperfusion injury through inducing NLRP3 lactylation. BMC Cardiovasc Disord 24: 651, 2024.
19. Luo L, Ma X, Kong D, Dai Y, Li T, Yu H, Liu J, Li M, Xu Y, Xiang G, *et al*: Multiomics integrated analysis and experimental validation identify TLR4 and ALOX5 as oxidative stress-related biomarkers in intracranial aneurysms. J Neuroinflammation 21: 225, 2024.
20. Sheinberg DL, McCarthy DJ, Elwardany O, Bryant JP, Luther E, Chen SH, Thompson JW and Starke RM: Endothelial dysfunction in cerebral aneurysms. Neurosurg Focus 47: E3, 2019.
21. Uchida K, Yasunaga H, Sumitani M, Horiguchi H, Fushimi K and Yamada Y: Effects of remifentanil on in-hospital mortality and length of stay following clipping of intracranial aneurysm: A propensity score-matched analysis. J Neurosurg Anesthesiol 26: 291-298, 2014.
22. Ling C, Yang Y, Hu X, Cai M, Wang H and Chen C: Phoenixin-14 alleviates inflammatory smooth muscle cell-induced endothelial cell dysfunction in vitro. Cytokine 157: 155973, 2022.
23. Livak KJ and Schmittgen TD: Analysis of relative gene expression data using real-time quantitative PCR and the 2(-Delta Delta C(T)) method. Methods 25: 402-408, 2001.
24. Glancy B, Kane DA, Kavazis AN, Goodwin ML, Willis WT and Gladden LB: Mitochondrial lactate metabolism: History and implications for exercise and disease. J Physiol 599: 863-888, 2021.
25. Wu J, Gu X, Zhang J, Mi Z, He Z, Dong Y, Ge W, Ghimire K, Rong P, Wang W and Ma X: 4-OI Protects MIN6 cells from oxidative stress injury by reducing LDHA-Mediated ROS generation. Biomolecules 12: 1236, 2022.
26. Bonafiglia QA, Bendeck M and Gotlieb AI: Vascular pathobiology: Atherosclerosis and large vessel disease. Cardiovascular Pathology, Elsevier, pp65-306, 2022.
27. Morel S, Schilling S, Diagbouga MR, Delucchi M, Bochaton-Piallat ML, Lemeille S, Hirsch S and Kwak BR: Effects of low and high aneurysmal wall shear stress on endothelial cell behavior: Differences and similarities. Front Physiol 12: 727338, 2021.
28. Zhu H, Zeng Y, Tan J, Li M and Zhao Y: HMGB1 induced oxidative stress and Inflammation in endothelial cells exposed to Impinging Flow. Cerebrovasc Dis 53: 437-48, 2024.
29. Mustafa M, Ahmad R, Tantry IQ, Ahmad W, Siddiqui S, Alam M, Abbas K, Moinuddin, Hassan MI, Habib S and Islam S: Apoptosis: A comprehensive overview of signaling pathways, morphological changes, and physiological significance and therapeutic implications. Cells 13: 1838, 2024.
30. Huang J, Hong L, Shen B, Zhou Y, Lan J and Peng Y: FOXO1 represses MCL1 transcription to regulate the function of vascular smooth muscle cells in intracranial aneurysm. Exp Brain Res 240: 2861-2870, 2022.
31. Kowalczyk P, Sulejczak D, Kleczkowska P, Bukowska-Ośko I, Kucia M, Popiel M, Wietrak E, Kramkowski K, Wrzosek K and Kaczyńska K: Mitochondrial oxidative stress-A causative factor and therapeutic target in many diseases. Int J Mol Sci 22: 13384, 2021.
32. Tavris BS, Peters AS, Böckler D and Dihlmann SL: Mitochondrial dysfunction and increased DNA damage in vascular smooth muscle cells of abdominal aortic aneurysm (AAA-SMC). Oxid Med Cell Longev 2023: 6237960, 2023.
33. Nguyen A, Patel AB, Kioutchoukova IP, Diaz MJ and Lucke-Wold B: Mechanisms of mitochondrial oxidative stress in Brain Injury: From pathophysiology to therapeutics. Oxygen 3: 163-178, 2023.
34. Chen B, Xie K, Zhang J, Yang L, Zhou H, Zhang L and Peng R: Comprehensive analysis of mitochondrial dysfunction and necroptosis in intracranial aneurysms from the perspective of predictive, preventative, and personalized medicine. Apoptosis 28: 1452-1468, 2023.
35. Zhang H, Liu X, Yang F, Cheng D and Liu W: Overexpression of HIF-1α protects PC12 cells against OGD/R-evoked injury by reducing miR-134 expression. Cell Cycle 19: 990, 2020.
36. Yfantis A, Mylonis I, Chachami G, Nikolaidis M, Amoutzias GD, Paraskeva E and Simos G: Transcriptional response to hypoxia: The role of HIF-1-associated co-regulators. Cells 12: 798, 2023.
37. Lee SH, Golinska M and Griffiths JR: HIF-1-independent mechanisms regulating metabolic adaptation in hypoxic cancer cells. Cells 10: 2371, 2021.
38. Kalashnyk O, Lykhmus O, Koval L, Uspenska K, Obolenskaya M, Chernyshov V, Komisarenko S and Skok M: α7 Nicotinic acetylcholine receptors regulate translocation of HIF-1α to the cell nucleus and mitochondria upon hypoxia. Biochem Biophys Res Commun 657: 35-42, 2023.
39. Papandreou I, Cairns RA, Fontana L, Lim AL and Denko NC: HIF-1 mediates adaptation to hypoxia by actively downregulating mitochondrial oxygen consumption. Cell metabolism 3: 187-197, 2006.
40. Han Y, Li G, Zhang Z, Zhang X, Zhao B and Yang H: Axl promotes intracranial aneurysm rupture by regulating macrophage polarization toward M1 via STAT1/HIF-1α. Front Immunol 14: 1158758, 2023.
41. Gusdon AM, Fu C, Putluri V, Paz AS, Chen H, Ren X, Hassan MK, Dash P, Coarfa C, Putluri N, *et al*: Early systemic glycolytic shift after aneurysmal subarachnoid hemorrhage is associated with functional outcomes. Neurocrit Care 37: 724-734, 2022.
42. Dai M, Wang L, Yang J, Chen J, Dou X, Chen R, Ge Y and Lin Y: LDHA as a regulator of T cell fate and its mechanisms in disease. Biomed Pharmacother 158: 114164, 2023.
43. Tian Q, Li J, Wu B, Wang J, Xiao Q, Tian N, Yi L, Luo M, Li Z, Pang Y, *et al*: Hypoxia-sensing VGLL4 promotes LDHA-driven lactate production to ameliorate neuronal dysfunction in a cellular model relevant to Alzheimer's disease. FASEB J 37: e23290, 2023.
44. Yin YL, Wang HH, Gui ZC, Mi S, Guo S, Wang Y, Wang QQ, Yue RZ, Lin LB, Fan JX, *et al*: Citronellal attenuates oxidative Stress-induced mitochondrial damage through TRPM2/NHE1 pathway and effectively inhibits endothelial dysfunction in type 2 diabetes mellitus. Antioxidants 11: 2241, 2022.
45. Gupta R, Gupta N, Gupta R and Gupta N: Glycolysis and gluconeogenesis. Fund Bacterial Physiol Metabol: 267-87, 2021.
46. Zhao Y, Zhang J, Zheng Y, Zhang Y, Zhang XJ, Wang H, Du Y, Guan J, Wang X and Fu J: NAD+ improves cognitive function and reduces neuroinflammation by ameliorating mitochondrial damage and decreasing ROS production in chronic cerebral hypoperfusion models through Sirt1/PGC-1α pathway. J Neuroinflammation 18: 207, 2021.
47. Lee MJ, Zhu J, An J, Choi HJ, Pyo CH and Heo JY: The increase of Nad/Nadh ratio in mitochondria alleviates intracerebral hemorrhage injury by enhancing neurovascular unit integrity. IBRO Neurosci Rep 15: S598, 2023.

48. Zhang J, Duan P, Nie B, Zhang Z, Shi R, Liu Q, Wang S, Xu T and Tian J: Identification and verification of the oxidative Stress-related signature markers for intracranial Aneurysm-applied bioinformatics. Front Biosci (Landmark Ed) 29: 294, 2024.
49. Mondal A, Mukherjee S, Upadhyay P, Saxena I, Pati S and Singh S: Enhancing NADPH to restore redox homeostasis and lysosomal function in G6PD-deficient microglia. bioRxiv 2024: 607918, 2024.
50. Mondal A, Munan S, Saxena I, Mukherjee S, Upadhyay P, Gupta N, Dar W, Samanta A, Singh S and Pati S: G6PD deficiency mediated impairment of iNOS and lysosomal acidification affecting phagocytotic clearance in microglia in response to SARS-CoV-2. Biochim Biophys Acta Mol Basis Dis 1870: 167444, 2024.
51. Wiśniewski K, Popęda M, Price B, Bieńkowski M, Fahlström A, Drummond K and Adamides AA: Glucose-6-phosphate dehydrogenase and 8-iso-prostaglandin F2α as potential predictors of delayed cerebral ischemia after aneurysmal subarachnoid hemorrhage. J Neurosurg 139: 698-707, 2023.
52. Zhang YM, Miao ZM, Chen YP, Song ZB, Li YY, Liu ZW, Zhou GC, Li J, Shi LL, Chen Y, *et al*: Ononin promotes radiosensitivity in lung cancer by inhibiting HIF-1α/VEGF pathway. Phytomedicine 125: 155290, 2024.
53. Li PP, He L, Zhang LM, Qin XM and Hu JP: Naoluo xintong decoction ameliorates cerebral Ischemia-reperfusion injury by promoting angiogenesis through activating the HIF-1α/VEGF signaling pathway in rats. Evid Based Complement Alternat Med 2022: 9341466, 2022.
54. Chen J, Zhang M, Liu Y, Zhao S, Wang Y, Wang M, Niu W, Jin F and Li Z: Histone lactylation driven by mROS-mediated glycolytic shift promotes hypoxic pulmonary hypertension. J Mol Cell Biol 14: mjac073, 2023.
55. Ai X, Yu P, Luo L, Sun J, Tao H, Wang X and Meng X: Berberis dictyophylla F. inhibits angiogenesis and apoptosis of diabetic retinopathy via suppressing HIF-1α/VEGF/DLL-4/Notch-1 pathway. J Ethnopharmacol 296: 115453, 2022.
56. Lee DC, Sohn HA, Park ZY, Oh S, Kang YK, Lee KM, Kang M, Jang YJ, Yang SJ, Hong Y, *et al*: A Lactate-induced response to hypoxia. Cell 161: 595-609, 2015.